

# Occupant Preference-Aware Load Scheduling for Resilient Communities

Jing Wang<sup>a</sup>, Sen Huang<sup>b</sup>, Wangda Zuo<sup>a,c,\*</sup>, Draguna Vrabić<sup>b</sup>

<sup>a</sup> University of Colorado Boulder, Department of Civil, Environmental and Architectural  
Engineering, Boulder, CO 80309, United States

<sup>b</sup> Pacific Northwest National Laboratory, 902 Battelle Blvd, Richland, WA 99354, United States

<sup>c</sup> National Renewable Energy Laboratory, 15013 Denver West Parkway, Golden, CO 80401,  
United States

## Abstract

The load scheduling of resilient communities in the islanded mode is subject to many uncertainties such as weather forecast errors and occupant behavior stochasticity. To date, it remains unclear how occupant preferences affect the effectiveness of the load scheduling of resilient communities. This paper proposes an occupant preference-aware load scheduler for resilient communities operating in the islanded mode. The load scheduling framework is formulated as a model predictive control problem. Based on this framework, a deterministic load scheduler is adopted as the baseline. Then, a chance-constrained scheduler is proposed to address the occupant-induced uncertainty in room temperature setpoints. Key resilience indicators are selected to quantify the impacts of the uncertainties on community load scheduling. Finally, the proposed preference-aware scheduler is compared with the deterministic scheduler on a virtual testbed based on a real-world net-zero energy community in Florida, USA. Results show that the proposed scheduler performs better in terms of serving the occupants' thermal preference and reducing the required

---

\* Corresponding author.  
Email address: wangda.zuo@colorado.edu.

22 battery size, given the presence of the assumed stochastic occupant behavior. This work indicates  
 23 that it is necessary to consider the stochasticity of occupant behavior when designing optimal load  
 24 schedulers for resilient communities.

25 **Keywords:** Microgrid; Optimal load scheduling; Uncertainty; Occupant behavior; Resilient  
 26 community; Model predictive control.

27 **Nomenclature**

Parameters		$E_{bat}^t$	battery energy
$a$	intercept coefficient for the logistic regression model	$P_{ch}^t$	battery charging power
$b$	slope coefficient for the logistic regression model	$P_{crit,j}^t$	scheduled critical loads
$\bar{E}_{bat}$	upper limit of battery energy	$P_{curt}^t$	curtailed PV power
$e$	mathematical constant	$P_{dis}^t$	battery discharging power
H	MPC prediction horizon	$P_{hvac}^t$	HVAC system (heat pump) total power
N	simulation horizon	$P_{load}^t$	total scheduled loads
$N_{crit}$	number of critical loads in each building	$P_{modu,j}^t$	scheduled modulatable loads
$N_{modu}$	number of modulatable loads in each building	$P_{shed,j}^t$	scheduled sheddable loads
$N_{shed}$	number of sheddable loads in each building	$P_{shif,j}^t$	scheduled shiftable loads
$N_{shif}$	number of shiftable loads in each building	$P_{pv}^t$	PV power
$n_{shif,j}$	average cycle time of each shiftable load	$r_{hvac}^t$	speed ratio of the heat pump
$\bar{P}_{bat}$	upper limit of battery power	$T_{room}$	indoor air temperature
$\hat{P}_{crit,j}^t$	critical load data	$t_{shif,j,s}$	starting operation time of shiftable loads
$P_{hvac,nom}$	HVAC system (heat pump) nominal power	$Q_{gain}^t$	internal heat gain
$\bar{P}_{load}^t$	predicted loads upper bound	<b>Binary Variables</b>	
$\hat{P}_{modu,j}^t$	modulatable load data	$u_{shed,j}^t$	binary decision variable for sheddable load on/off status
$\hat{P}_{shed,j}^t$	sheddable load data	$v_{shif,j}^t$	binary variable for shiftable load starting time
$P_{shif,j,avg}$	average nominal power of each shiftable load	<b>Abbreviations</b>	
$p$	probability of setpoint-changing actions	BAL	building agent layer
$\mathbf{S}_{shif,j}$	scheduling matrix for each shiftable load	CDF	cumulative distribution function
$T_{amb}^t$	ambient outdoor temperature	COL	community operator layer
$T_{room}$	lower room temperature bound	DER	distributed energy resource

$\bar{T}_{room}$	upper room temperature bound	DR	demand response
$Q_{sol}^t$	solar irradiance	HVAC	heating, ventilation, and air-conditioning
$\gamma$	penalty coefficients	KRI	key resilience indicator
$\Delta t$	timestep	MPC	model predictive control
$\epsilon, \epsilon_T$	maximum constraint violation probability	RC	resistance-capacitance
$\eta_{ch}$	battery charging efficiency	RMSE	Root Mean Square Error
$\eta_{dis}$	battery discharging efficiency	SOC	state of charge
$\mu_T^t$	mean of room temperature error distribution	PDF	probability density function
$\sigma_T^t$	standard deviation of room temperature error distribution	PID	proportional integral derivative
<b>Continuous Variables</b>		PV	photovoltaics

28

## 29 1 Introduction

30 Due to the increasing frequency of extreme weather events such as the 2021 Texas Power Crisis  
31 [1], there is an emerging need for community resilience studies. Resilient communities refer to  
32 those that can sustain disruptions and adapt to them quickly by continuing to operate without  
33 sacrificing the occupants' essential needs [2, 3]. Enabling technologies for resilient communities  
34 often involve distributed energy resources (DERs) such as photovoltaics (PV) and electrical energy  
35 storage (EES) systems. When disconnected from the main grid, the adoption of advanced control  
36 techniques can help enhance community resilience.

37 As an advanced control technique, optimal load scheduling determines the operation schedules of  
38 controllable devices in the community to achieve optimization objectives. For a resilient  
39 community, typical controllable assets include the EES, PV, and thermostatically controllable  
40 devices in buildings such as the heating, ventilation, and air-conditioning (HVAC) system.  
41 Building plug loads that are sheddable, shiftable, or modulatable can also be considered flexible  
42 loads in islanded circumstances [4]. The objectives of the load scheduling for resilient

43 communities often involve maximizing the self-consumption rate of locally generated PV energy,  
44 minimizing PV curtailment, and minimizing the unserved ratio to critical loads.

45 It is important to account for uncertainties when designing a load scheduler for resilient  
46 communities. Moreover, due to the limited amount of available PV generation during off-grid  
47 scenarios, the uncertainties need to be more carefully dealt with to ensure a satisfying control  
48 performance. Sources of uncertainties for a community load scheduling problem mainly lie in two  
49 aspects: power generation and consumption. For renewable energy generation, weather forecast  
50 errors play a prominent role in the cause of uncertainty. Whereas, for energy consumption,  
51 occupant behavior stochasticity is a major source of uncertainty.

52 Much of existing load scheduling research has considered the uncertainty of weather forecasts [5–  
53 13]. Kou [5] proposed a comprehensive scheduling framework for residential building demand  
54 response (DR) considering both day-ahead and real-time electricity markets. The results  
55 demonstrated the effectiveness of the proposed approach for large-scale residential DR  
56 applications under weather and consumer uncertainties. Garifi [13] adopted stochastic  
57 optimization in a model predictive control (MPC)-based home energy management system. The  
58 indoor thermal comfort is ensured at a high probability with uncertainty in the outdoor temperature  
59 and solar irradiance forecasts. Faraji [6] proposed a hybrid learning-based method using an  
60 artificial neural network to precisely predict the weather data, which eliminated the impact of  
61 weather forecast uncertainties on the scheduling of microgrids. Similarly, in the authors' previous  
62 publication [7], normally distributed outdoor temperature and solar irradiance forecast errors were  
63 introduced into the community control framework, which accounted for the uncertainties in the  
64 weather forecasts.

65 However, the uncertainties from the power consumption perspective, especially the occupant  
66 behavior uncertainty, is rarely accounted for in load scheduling research [14–18]. Some efforts to  
67 integrate occupant behavior modeling can be found in studies of building optimal control [19–22].  
68 Aftab [19] used video-processing and machine-learning techniques to enable real-time building  
69 occupancy recognition and prediction. This further facilitated the HVAC system operation control  
70 to achieve building energy savings. Lim [20] solved a joint occupancy scheduling and occupancy-  
71 based HVAC control problem for the optimal room-booking (i.e., meeting scheduling) in  
72 commercial and educational buildings. Both the occupancy status of each meeting room and the  
73 HVAC control variables were decision variables. Mixed-integer linear programming was adopted  
74 to optimally solve the optimization problem.

75 Notably, all of the preceding control work considered the stochasticity of building occupancy  
76 schedules, but the integration of other types of occupant behavior into building optimal control is  
77 not well studied in existing literature. Some researchers integrate the occupant thermal sensation  
78 feedback into the MPC for buildings [23, 24]. For instance, Chen [23] integrated a dynamic thermal  
79 sensation model into the MPC to help achieve energy savings using the HVAC control. For the  
80 occupant sensation model, the predictive performance of certainty-equivalence MPC and chance-  
81 constrained MPC were compared.

82 To summarize, the literature review shows that current research mainly focuses on the load  
83 scheduling of single buildings under grid-connected scenarios. There is a lack of research on the  
84 optimal load scheduling of resilient communities informed by occupant behavior uncertainties in  
85 the islanded mode. Given this gap, this paper proposes an occupant preference-aware load  
86 scheduling framework for resilient communities in the islanded mode. The occupants' thermal

87 preference for indoor air temperature will be reflected in the integration of thermostat adjustment  
88 probabilistic models. The optimal load scheduling is formulated as an MPC problem, so the  
89 stochastic thermostat-changing behavior will be regarded as the uncertainty in the MPC problem.  
90 Different methods, such as the offset-free method and robust method, can be used to handle the  
91 uncertainties in MPC problems [25]. The chance-constraint method, also known as the stochastic  
92 MPC, was selected to deal with the uncertainty in occupant preference in our study. It allows the  
93 violation of certain constraints at a predetermined probability. It thus enables a systematic trade-  
94 off between the control performance and the constraint violations [26]. The advantage of  
95 addressing occupant preference uncertainty by using the chance-constraint method lies in the *a*  
96 *priori* handling of the uncertainty, which does not require the extra error-prediction models needed  
97 by other methods (i.e., offset free method), and thus simplifies the control problem [27]. Therefore,  
98 less computational effort is required after the control design phase. Though it requires the  
99 controller to know the estimated uncertainty distribution beforehand, the development of occupant  
100 behavior probabilistic modeling will make knowing this less challenging.

101 In this work, we consider the load scheduling of a resilient community in islanded mode during  
102 power outages. The goal is to study the impact of occupants' thermal preference on the operation  
103 of an islanded community. The load scheduling problem of the community will be solved using  
104 an optimization-based hierarchical control framework. Occupant thermal preference will be  
105 integrated through thermostat changing behavioral models to inform the development of the load  
106 scheduler. The major contributions of this work include (1) a proposed new preference-aware load  
107 scheduler for resilient communities, which assures better control performance related to satisfying  
108 occupants' thermal preferences and reducing the battery size; (2) the quantification of the impact

109 of occupant thermostat-changing behavior on resilient community optimal scheduling using  
110 selected key resilience indicators (KRIs); and (3) the testing of the proposed scheduler on a high-  
111 fidelity virtual testbed for resilient communities.

112 The remainder of this paper is organized as follows: Section 2 details the research methodology.  
113 Section 3 describes the controllable device models used in this work involving the building HVAC  
114 models, load models, and battery models. Section 4 then discusses the deterministic versus  
115 stochastic scheduler formulations and proposes a chance-constrained controller for preference-  
116 aware load scheduling of resilient communities. Section 5 applies the theoretical work to a case  
117 study community and quantifies the impact of occupant preference uncertainty. Simulation results  
118 and discussions are presented in this section. Finally, Section 6 concludes the paper by identifying  
119 future work.

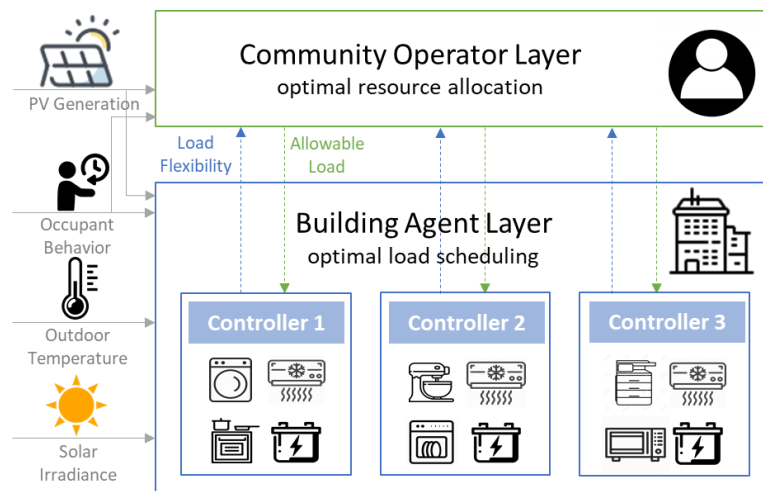
## 120 2 Methodology

121 In this section, we first introduce a hierarchical optimal control structure for resilient community  
122 load scheduling. Based on the structure, a deterministic scheduler will be implemented as the  
123 baseline. Further, we propose a research workflow to implement a stochastic preference-aware  
124 scheduler for addressing uncertainties in occupant thermostat-changing behavior. KRIs are  
125 proposed at the end of this section.

### 126 2.1 Hierarchical Optimal Control for Resilient Communities

127 In this study, we assume that the only energy resource accessible to the islanded community is on-  
128 site PV generation and the batteries for an extended period of more than 24 hours. In this problem  
129 setting, in order to make full use of the limited amount of PV generation and satisfy the occupants'  
130 essential needs, the building loads need to be shifted or modulated. The battery works as a temporal

131 arbitrage for meeting the demand at night. In addition, the occupant thermal preference will affect  
 132 the energy consumption of the HVAC system through the stochastic thermostat-changing behavior.  
 133 To optimally control such a community, considering the above factors, we adopted a hierarchical  
 134 control structure.  
 135 As illustrated in Figure 1, two layers of control are formulated: a community operator layer (COL)  
 136 and a building agent layer (BAL). The COL optimally allocates the limited amount of the on-site  
 137 PV generation based on the load flexibility provided by each building. The calculated allowable  
 138 load for each building is then passed down to the BAL, where each building optimally schedules  
 139 its controllable devices (i.e., HVAC, battery, and controllable loads) to achieve its local  
 140 optimization goals. Both layers are formulated as MPC-based optimization problems.



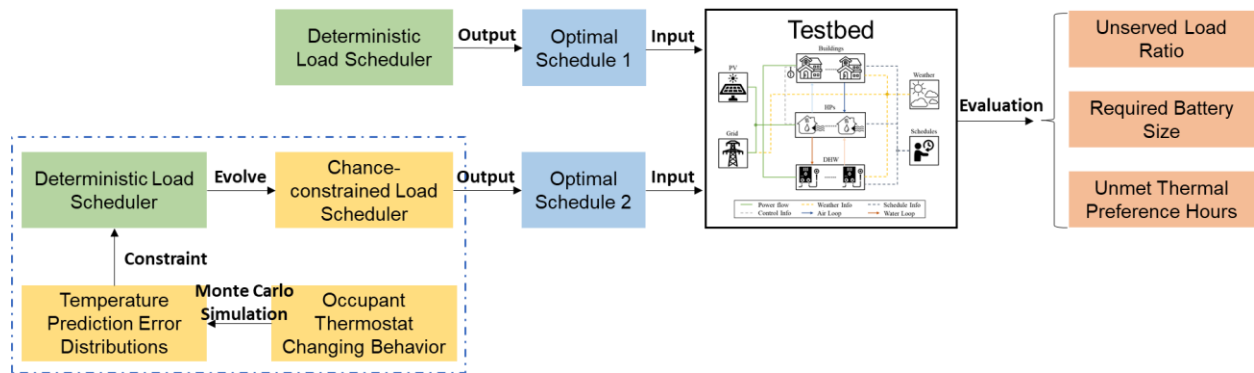
141  
 142 *Figure 1 The hierarchical optimal control structure for community operation.*

143 The input of the hierarchical control involves the predicted PV generation data, outdoor air dry-  
 144 bulb temperature, and solar irradiance. The PV generation data are used by the COL to determine  
 145 the optimal allocation among buildings. The temperature and irradiance data are used by the  
 146 HVAC models for updating the indoor room temperature predictions. The occupant behavior

147 affects the two layers differently. The COL uses building occupancy schedules to decide the  
 148 weights of different buildings during the PV allocation (details can be found in [7]). The BAL  
 149 considers occupant thermal preference to be the uncertainty in the indoor room temperature  
 150 prediction.

151 **2.2 Proposed Workflow**

152 Figure 2 depicts the workflow of this paper. A deterministic optimal load scheduler without the  
 153 occupant thermal preference uncertainty is implemented in the hierarchical control structure.  
 154 Further, to account for the uncertainties, we propose a chance-constrained controller. It is  
 155 developed based on the deterministic controller and involves an alteration of the room temperature  
 156 constraints, which accounts for the uncertainties in room temperature prediction errors caused by  
 157 the occupants' thermostat-changing behavior. The Monte Carlo simulation method was adopted  
 158 to cover a wide range of simulation results.



160 *Figure 2 Diagram of the proposed workflow.*

161 Further, to reflect various styles of occupant behavior, three types of occupant thermostat-changing  
 162 models were adopted: low, medium, and high, which represent three levels of frequencies of the  
 163 thermostat-changing activities. Here, we assume that when the occupant decides to change the

164 indoor air temperature setpoint according to their preference, the predetermined optimal HVAC  
 165 equipment control setting at the current timestep will be overridden. Instead, a new control setting  
 166 will be calculated to achieve the occupants' setpoint at the current timestep. At the next timestep,  
 167 the predetermined optimal setting will still be used if the occupant is not changing the setpoint  
 168 consecutively.

169 Finally, the optimal schedules determined by the chance-constrained controller and the  
 170 deterministic controller are tested on a high-fidelity virtual testbed [28] with respect to their  
 171 individual performances. KRIs such as the unserved load ratio, the required battery size, and the  
 172 unmet thermal preference hours were adopted to quantify the results.

173 The *unserved load ratio* in this paper is defined as the relative discrepancy between the served  
 174 load  $P_{load}^t$  and the originally predicted load  $\bar{P}_{load}^t$ :

$$Unserved\ load\ ratio = \frac{\sum_{t=1}^N (\bar{P}_{load}^t - P_{load}^t)}{\sum_{t=1}^N \bar{P}_{load}^t}, \quad (1)$$

175 where  $N$  is the MPC simulation horizon of 48 hours. The *required battery size* is obtained by  
 176 subtracting the minimum battery SOC from the maximum SOC. This gives us a sense of how much  
 177 of the battery capacity has been used under different scenarios. Finally, we define the *unmet*  
 178 *thermal preference hours* metric for the cumulative absolute difference between the actual and the  
 179 preferred room temperature over the optimization horizon:

$$Unmet\ thermal\ preference\ hours = \sum_{t=1}^N |T_{room}^t - T_{prefer}^t| \Delta t. \quad (2)$$

180 It quantifies how well the controller performs to satisfy the occupants' thermal preference and has  
 181 the unit of °C·h (degree hours).

## 182 3 Models for Controllable Devices

### 183 3.1 HVAC Models

184 This study assumes that heating and cooling is provided by heat pumps and the heat pump energy  
185 consumption represents the HVAC system energy consumption. We adopted linear regression  
186 models for the HVAC system to predict room temperatures at each timestep. To precisely model  
187 the building thermal reactions, two types of parameters that contribute to the heat gain of the  
188 building space are considered. The first type is environmental parameters such as the outdoor air  
189 dry-bulb temperature and solar irradiance. The second type represents the internal heat gain due to  
190 the presence of the occupants and the operation of appliances. We assumed that the simulated  
191 buildings are well sealed and thus the interference from the infiltration can be omitted. Therefore,  
192 the HVAC model updates the indoor room temperature based on the room temperature at the last  
193 timestep, the abovementioned heat gains, and the heating/cooling provided by the heat pump  
194 system at every timestep. The control variable is the heat pump speed ratio, which ranges from 0  
195 to 1 continuously. The resulting HVAC power is equal to the speed ratio multiplied by the nominal  
196 heat pump power. Additionally, to better account for the effect of building thermal mass, for each  
197 heat gain parameter, two past terms are adopted, respectively [29]. The equations for the HVAC  
198 model are as follows:

$$T_{room}^{t+1} = \beta_1 T_{room}^t + \beta_2 T_{room}^{t-1} + \beta_3 T_{amb}^t + \beta_4 T_{amb}^{t-1} + \beta_5 r_{hvac}^t + \beta_6 Q_{sol}^t + \beta_7 Q_{sol}^{t-1} + \beta_8 Q_{gain}^t + \beta_9 Q_{gain}^{t-1} \quad (3)$$

$$\text{s.t. } 0 \leq r_{hvac}^t \leq 1, \quad (4)$$

$$P_{hvac}^t = r_{hvac}^t P_{hvac,nom}, \quad (5)$$

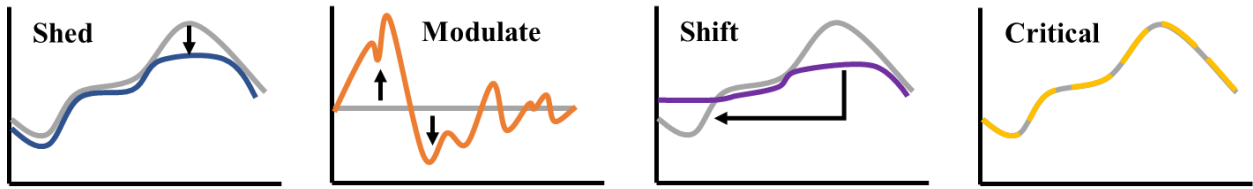
199 where  $T_{room}^t$ ,  $T_{amb}^t$ ,  $Q_{sol}^t$ , and  $Q_{gain}^t$  represent the room temperature, ambient dry-bulb temperature,  
200 solar irradiance, and internal heat gain at timestep  $t$ , respectively. The  $r_{hvac}^t$  and  $P_{hvac,nom}$  are the  
201 heat pump speed ratio and the nominal HVAC system power. The linear regression coefficients  
202 are represented by  $\beta$ . For  $\beta_5$ , a negative value means cooling and positive means heating.

203 In the model,  $Q_{gain}^t$  and  $Q_{gain}^{t-1}$  are related to the occupant presence and the operation of the  
204 building appliances. When the building is occupied, 70% of the total heat rate of a person (i.e.,  
205 100 W) is dissipated as sensible heat into the space and the rest 30% is latent heat [30]. The heat  
206 gain from appliances is calculated by the power of the appliance multiplied by its heat gain  
207 coefficient, which reflects how much of the consumed electric power is dissipated into the space  
208 as heat. Table A-1 in Appendix A lists the heat gain coefficients adopted from literature [31–33].  
209 Note that the controllable loads are optimization variables of the scheduling problem, which will  
210 be iteratively calculated at each optimization timestep. Therefore, to speed up the optimization, we  
211 reduced the coupling between the thermal models and the electric demand models. This was done  
212 by calculating the weighted average heat gain coefficients for each building based on the capacity  
213 of each appliance (Table A-1).

### 214 3.2 Load and Battery Models

215 The building load models in this work are categorized into four types according to their power  
216 flexibility characteristics: sheddable, modulatable, shiftable, and critical (Figure 3). We did the  
217 categorization from the perspective of the building owners during power outages. The sheddable  
218 loads are those that can be disconnected without affecting the occupants' essential needs. For  
219 instance, the microwave in a bakery is categorized as sheddable during an outage. The modulatable  
220 loads are the systems that have varying power shapes such as an HVAC system with a variable

221 frequency drive. The shiftable loads are the appliances that have flexible operation schedules such  
 222 as washers and dryers. Lastly, the critical loads refer to appliances and systems related to the  
 223 occupants' essential needs. In this work, we consider only loads used for lighting and food  
 224 preservation as critical loads, which aligns with the two bottom levels of Maslow's Hierarchy of  
 225 Needs (i.e., physiological and safety needs) [34]. The critical loads account for about 20% to 90%  
 226 of the total building loads depending on building type and time of day.



227  
 228 *Figure 3 Power flexibility characteristics of the four load types [35].*

229 The mathematical formulation of the sheddable load is shown in Equation (6):

$$P_{shed,j}^t = u_{shed,j}^t \hat{P}_{shed,j}^t, \quad j \in \{1, \dots, N_{shed}\}, \quad (6)$$

230 where  $u_{shed,j}^t$  is a binary optimization variable,  $\hat{P}_{shed,j}^t$  is the original sheddable load time series  
 231 data, and  $N_{shed}$  is the number of sheddable loads in the building. The actual sheddable load after  
 232 optimization  $P_{shed,j}^t$  is determined by the ON/OFF status represented by the binary variable. The  
 233 modulatable load  $P_{modu,j}^t$  is formulated as a continuous optimization variable, which ranges  
 234 between zero and its original power demand  $\hat{P}_{modu,j}^t$ . Equation (7) sets the lower and upper bound  
 235 of the modulatable load.

$$0 \leq P_{modu,j}^t \leq \hat{P}_{modu,j}^t, \quad j \in \{1, \dots, N_{modu}\}. \quad (7)$$

236 The shiftable loads are scheduled through scheduling matrices [36]. First, using the power data  
 237 [37], we extracted the average cycle time  $n_{shif,j}$  and the average power demand  $P_{shif,j,avg}$  of each

238 shiftable load. The starting operation timestep  $t_{shif,j,s}$  of each shiftable load is optimized over the  
 239 MPC horizon. At the scheduled starting timestep, the binary variable  $v_{shed,j}^t$  equals 1 and is 0  
 240 otherwise:

$$v_{shif,j}^t = \begin{cases} 1, & t = t_{shif,j,s}, \\ 0, & t \neq t_{shif,j,s}, \end{cases} \quad (8)$$

$$\forall t \in \{1, \dots, H - n_{shif,j} + 1\}, \quad j \in \{1, \dots, N_{shif}\}.$$

241  $H$  is the MPC prediction horizon. Once the starting time of a shiftable load is selected, the power  
 242 demand of the load is then fixed at its average power until it finishes its cycle. The appliance must  
 243 finish its cycle before the horizon ends ( $t \in \{1, \dots, H - n_{shif,j} + 1\}$ ). Here, we assume that each  
 244 shiftable load operates once and only once during each horizon, which is enforced by:

$$\sum_{t=1}^{H-n_{shif,j}+1} v_{shif,j}^t = 1. \quad (9)$$

245 Next, a scheduling matrix  $\mathbf{S}_{shif,j}$  of shape  $H \times (H - n_{shif,j} + 1)$  is generated for each shiftable  
 246 load. The actual power shape of the load, denoted  $P_{shif,j}^t$ , is thus calculated by:

$$P_{shif,j}^t = \mathbf{S}_{shif,j} \times \begin{bmatrix} v_{shif,j}^1 \\ \vdots \\ v_{shif,j}^{H-n_{shif,j}+1} \end{bmatrix} \times P_{shif,j,avg}. \quad (10)$$

247 Finally, the actual critical load  $P_{crit,j}^t$  must be exactly equal to the critical power demand  $\hat{P}_{crit,j}^t$ ,  
 248 as enforced by:

$$P_{crit,j}^t = \hat{P}_{crit,j}^t, \quad j \in \{1, \dots, N_{crit}\}. \quad (11)$$

249 Summing up the four types of loads in each building, we obtain the optimization variable  $P_{load}^t$  as  
 250 follows:

$$P_{load}^t = \sum_{j=1}^{N_{shed}} P_{shed,j}^t + \sum_{j=1}^{N_{modu}} P_{modu,j}^t + \sum_{j=1}^{N_{shif}} P_{shif,j}^t + \sum_{j=1}^{N_{crit}} P_{crit,j}^t. \quad (12)$$

251 The linear battery model adopted in this work is represented by Equation (13). The battery state of  
 252 charge (SOC)  $E_{bat}^{t+1}$  is predicted based on the SOC of the previous timestep  $E_{bat}^t$ , the battery  
 253 charging  $P_{ch}^t$  or discharging power  $P_{dis}^t$  at each step, and the battery charging/discharging  
 254 efficiencies  $\eta_{ch}$  and  $\eta_{dis}$ . The inequality constraints in Equations (14) and (15) enforce the  
 255 acceptable limits for the battery charging/discharging power and SOC, where  $\bar{P}_{bat}$  and  $\bar{E}_{bat}$  are  
 256 the maximum values for battery power and capacity:

$$E_{bat}^{t+1} = E_{bat}^t + \eta_{ch} P_{ch}^t \Delta t - \frac{1}{\eta_{dis}} P_{dis}^t \Delta t, \quad (13)$$

$$\text{s.t. } 0 \leq P_{ch}^t, P_{dis}^t \leq \bar{P}_{bat}, \quad (14)$$

$$0 \leq E_{bat}^{t+1} \leq \bar{E}_{bat}. \quad (15)$$

## 257 4 Optimal Load Scheduling

258 This section first presents the mathematical formulation of the deterministic load scheduler. After  
 259 that, we will introduce the formulation of the occupant preference-aware stochastic scheduler  
 260 containing three parts: the thermostat-changing model, the uncertainty introduction mechanism,  
 261 and the method to address the uncertainty.

### 262 4.1 Deterministic Scheduler

263 As introduced in Section 2.1, the deterministic scheduler adopts a two-layer structure with COL  
 264 and BAL. The objective of the COL is to minimize the community-level PV curtailment to  
 265 facilitate better use of the limited PV power during the outage. The main constraints are the load  
 266 flexibility of each building, building occupancy, and building priority, etc. No detailed building  
 267 assets are simulated at the community layer. This ensures that the COL is computationally tractable,

268 especially when the problem scales up and the number of controllable building assets scales up.  
 269 The detailed mathematical formulation of the COL can be found in reference [7].  
 270 The objective of the BAL is to minimize the unserved load ratio of each building within the  
 271 allowable load range allocated by the COL. This is achieved through MPC-based optimal  
 272 scheduling of the building-owned HVAC system, controllable loads, and battery. The optimization  
 273 is a mixed-integer linear programming problem, because the sheddable and shiftable load models  
 274 contain binary variables. Next, the mathematical formulation of the optimization problem is  
 275 presented. Note that the formulation applies for every individual building in the community.  
 276 The cost function to minimize the unserved load ratio is formulated as:

$$f_{cost}(t, \{x^t\}_{t=1}^H) = \sum_{t=1}^H (\bar{P}_{load}^t - P_{load}^t) + \sum_{t=1}^H \gamma P_{ch}^t + \sum_{t=1}^H \gamma' P_{curt}^t, \quad (16)$$

$$\min_{\{x^t\}_{t=1}^H} f_{cost}(t, \{x^t\}_{t=1}^H), \quad (17)$$

277 where  $\bar{P}_{load}^t$  is the predicted load upper bound from data. The difference between this upper bound  
 278 and the actual operated loads  $P_{load}^t$  is minimized to achieve a maximum served load to the building.  
 279 To avoid simultaneous battery charging and discharging as well as PV curtailment, the objective  
 280 function also includes small penalizations of charging  $\gamma P_{ch}^t$  and curtailment  $\gamma' P_{curt}^t$  [38], where  $\gamma$   
 281 and  $\gamma'$  are the penalization coefficients. The power balance of each building that must be satisfied  
 282 at each timestep is given by:

$$P_{pv}^t - P_{curt}^t = P_{ch}^t - P_{dis}^t + P_{load}^t + P_{hvac}^t, \quad (18)$$

283 where PV curtailment  $P_{curt}^t$  is limited by how much PV generation  $P_{pv}^t$  is available:

$$0 \leq P_{curt}^t \leq P_{pv}^t. \quad (19)$$

284 The left-hand side of Equation (18) represents power generation, whereas the right-hand side  
 285 represents consumption. The  $P_{ch}^t$  and  $P_{dis}^t$  stand for the battery charging and discharging power as  
 286 in Equation (13). The  $P_{load}^t$  and  $P_{hvac}^t$  are the total building loads and the HVAC power calculated  
 287 in Equations (12) and (5), respectively. To assure thermal comfort of the indoor environment, a  
 288 temperature constraint is given by:

$$\underline{T}_{room} \leq T_{room}^t \leq \bar{T}_{room}, \quad (20)$$

289 where  $\underline{T}_{room}$  and  $\bar{T}_{room}$  are the lower and upper room temperature bounds implemented as hard  
 290 constraints. The optimization variables in each building agent are collected in vector  $x^t$ :

$$x^t = \begin{bmatrix} \{P_{curt}^t\}_{t=1}^H, \{P_{ch}^t\}_{t=1}^H, \{P_{dis}^t\}_{t=1}^H, \{r_{hvac}^t\}_{t=1}^H, \{u_{shed,j}^t\}_{t=1}^H, \\ \{P_{modu,j}^t\}_{t=1}^H, \{v_{shif,j}^t\}_{t=1}^{H-n_{shif,j}+1}, \{T_{room}^t\}_{t=1}^H, \{E_{bat}^t\}_{t=1}^H \end{bmatrix}. \quad (21)$$

## 291 4.2 Stochastic Preference-aware Scheduler

292 To address the uncertainties of occupant thermal preference in the scheduling problem of resilient  
 293 communities, this section introduces the stochastic preference-aware scheduler. First, we discuss  
 294 the modeling of the occupant behavior uncertainties as a probability function. Then we show the  
 295 mechanism by which this uncertainty might affect the optimal control of the HVAC system. After  
 296 that, we propose using the chance-constraint method to address the uncertainty.

### 297 4.2.1 Stochastic Thermostat-Changing Model

298 The stochastic occupant thermostat-changing model adopted in this paper was proposed by Gunay  
 299 et al. [39]. Through continuous observation of the occupants' thermostat keypress actions in

300 private office spaces, the relationship between the thermostat-changing behavior and the  
301 concurrent occupancy, temperature, and relative humidity was analyzed. It was noted that the  
302 frequency of thermostat interactions (i.e., increasing or decreasing) can be approximated as a  
303 univariate logistic regression model with the indoor temperature as the independent predictor  
304 variable. Though the original data set was obtained from two office buildings, Gunay et al.  
305 generalized the study to understand occupants' thermostat user behavior and temperature  
306 preferences. Given the universality of their work, we have adapted their models based on our use  
307 cases. Note that occupants might have varied (e.g., higher) tolerance of indoor temperature during  
308 an emergency situation. The exact thresholds need further experimental study and validation,  
309 which is out of the scope of this work.

310 The thermostat-changing behavior models determine whether the occupants will change the  
311 setpoint temperature based on the concurrent indoor air temperature. The probability of increasing  
312 and decreasing the temperature setpoint is predicted with a logistic regression model:

$$p = \frac{1}{1 + e^{-(a+bT_{room})}} \quad (22)$$

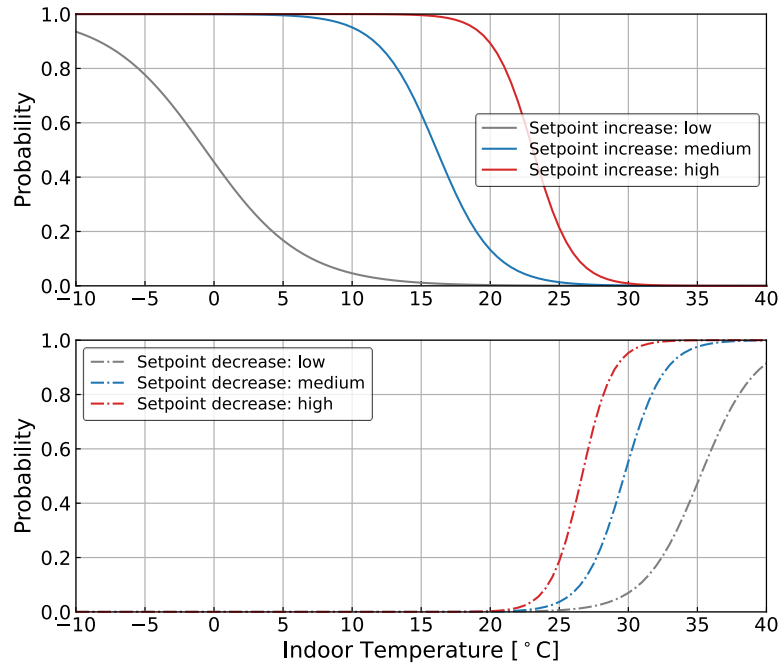
313 where  $p$  is the probability of the changing action,  $T_{room}$  is the indoor room temperature, and  $a$  and  
314  $b$  are coefficients. To investigate different uncertainty levels, we proposed three different active  
315 levels by revising the coefficients of the model in Equation (22). As shown in Table 1, the low  
316 active level adopts the original coefficients in [39]. Then, we proposed the medium and high active  
317 levels to represent various occupant thermal preference styles. The standard errors and p-values of  
318 the low active level coefficients are also provided in the table. As for the medium and high levels,  
319 we do not have measurement data for the statistical analysis since we adapted the coefficients from  
320 the original reference [39].

321 *Table 1 Coefficients in different active levels of the occupant thermostat-changing behavior*  
 322 *model.*

Active Level	Coefficients			
	Increasing		Decreasing	
	a	b	a	b
Low [39]	-0.179	-0.285	-17.467	0.496
Medium	7.821	-0.485	-20.667	0.696
High	15.821	-0.685	-23.867	0.896
Standard Error	1.047	0.048	0.684	0.028
p-value	0.864	0.000	0.000	0.000

323  
 324 Note that the adaptation of the original logistic regression models was made under the following  
 325 assumptions to ensure the adapted models remained realistic. For the setpoint increasing scenario,  
 326 the slope coefficient of *b* is varied linearly to reflect a higher frequency of the changing behavior.  
 327 The intercept coefficient *a* is then calculated to make sure that all active levels have the same value  
 328 of probability at the temperature of 40°C. For the setpoint decreasing scenario, a similar approach  
 329 is taken to make sure the same value of probability at 16°C is shared by all active levels. At each  
 330 thermostat interaction, we assume that 1°C of setpoint change would take place. Figure 4 depicts  
 331 the probabilities of the three active levels. Note that this figure contains a wider temperature range  
 332 than 16°C ~ 40°C to show a more comprehensive performance of the behavior models.

333



334

335

Figure 4 Probability of different thermostat-changing behavior.

336

Once the probability of the thermostat-changing behavior is determined using the above models,

337

the increasing or decreasing action is determined by comparing the probabilities with a randomly

338

generated number. At each optimization timestep, a random number between 0 and 1 is generated.

339

If the number is larger than  $1 - \Pr(\textit{increase})$ , the action will be to increase. On the contrary, if

340

it is smaller than  $\Pr(\textit{decrease})$ , the action will be to decrease. Because the sum of the increase

341

and decrease probabilities is smaller than 1 in our case, this algorithm assures at most one action

342

will be taken at each timestep.

343

#### 4.2.2 Introducing Occupant Behavior Uncertainties in Scheduling

344

To introduce the occupant thermostat-changing uncertainties to the load scheduling problem, a

345

stochastic simulation model representing the behavior needs to be incorporated into the

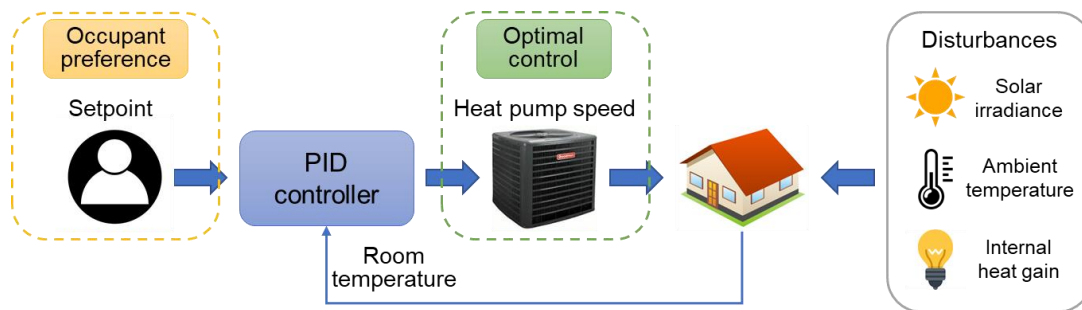
346

optimization. Figure 5 shows the control signal flow for the typical indoor air temperature control,

347

which affects the HVAC system operational status and its power consumption. The occupant sets

348 the temperature setpoint according to his/her preference through the thermostat. Behind the  
 349 thermostat, a proportional integral derivative (PID) controller decides the next heat pump speed to  
 350 offset the difference between the measured room temperature and the setpoint. This heat pump  
 351 speed signal is then fed into the heat pump system to provide cooling for the conditioned space.  
 352 Due to the presence of the dynamic environmental and behavioral disturbances, this process will  
 353 need to be repeated until the measured room temperature reaches the setpoint.



354  
 355 *Figure 5 Diagram showing the introduction of occupant thermostat-changing behavior to the*  
 356 *optimization.*

357 However, in the optimal control mechanism, the optimal scheduler takes over the control of the  
 358 heat pump speed from the PID controller. As a result, the occupants' preference has thus been  
 359 "disabled" to allow an optimal control determined by the scheduler. To mimic the overriding of  
 360 the room temperature setpoint by the occupants, the following algorithm was implemented in the  
 361 MPC problem and the pseudo code is shown below. Before each round of the optimization starts  
 362 (Steps 1–2), if the occupant decided to change the setpoint (Step 3), the heat pump speed for the  
 363 current timestep should be calculated to reach the setpoint instead of achieving the optimization  
 364 objective (Steps 4–7). Otherwise, the optimization runs normally because no overriding happens  
 365 (Step 7). After each optimization timestep, the flag variables indicating the thermostat-changing  
 366 actions need to be updated according to the concurrent room temperature (Step 8). It should be

367 noted that in the optimization, no PID controller has been implemented, so we assumed that  
 368  $T_{room}^t = T_{set}^t$  and the setpoint changes were directly added to the room temperature  $T_{room}^t$ .

<b>Step 1.</b> Start
<b>Step 2.</b> Initialization of flag variables: <i>increase</i> = <i>false</i> , <i>decrease</i> = <i>false</i> ;
<b>Step 3.</b> If <i>increase</i> = <i>true</i> or <i>decrease</i> = <i>true</i> : <div style="margin-left: 40px;"><b>Step 4</b> <math>T_{room}^t = T_{room}^{t-1} + 1</math> or <math>T_{room}^t = T_{room}^{t-1} - 1</math>;</div> <div style="margin-left: 40px;"><b>Step 5</b> Calculate the corresponding <math>r_{hvac}^t</math>;</div> <div style="margin-left: 40px;"><b>Step 6</b> Disable <math>r_{hvac}^t</math> from the optimization variables;</div>
<b>Step 7.</b> Run MPC for timestep $t$ ;
<b>Step 8.</b> Update flag variables (i.e., <i>increase</i> and <i>decrease</i> ) according to $T_{room}^t$ ;
<b>Step 9.</b> Repeat Steps 3–8 until the end of the MPC horizon of 48 hours;
<b>Step 10.</b> End

### 369 4.2.3 Chance-Constraint Method

370 As mentioned in Section 4.2.1, the uncertainties in the occupants' thermostat-changing behavior  
 371 are a probability function. In the scheduling optimization problem, the constraint directly affected  
 372 by the occupants' thermostat-changing behavior is the room temperature bounds. The uncertainties  
 373 related to the occupants' adjusting the thermostat could lead to the violation of the temperature  
 374 bounds during the implementation of the developed control strategies. Furthermore, this could lead  
 375 to other control-related performances being affected, including higher building load unserved ratio  
 376 and larger required battery size. To address this, we adopted the chance-constraint method.

377 By definition, the chance constraint allows the violation of a certain constraint with a small  
 378 probability, which thus presents a systematic trade-off between control performance and  
 379 probability of constraint violations [40]. It can be expressed in general by the following equation:

$$Pr(g(x, \xi) \leq 0) \geq 1 - \epsilon, \quad (23)$$

380 where  $g(x, \xi) \leq 0$  is the inequivalent constraint and  $\epsilon$  is the maximum violation probability.  
 381 Given the uncertainties in the occupants' thermostat-changing behavior, we assume that the  
 382 temperature bounds can be satisfied with a probability of  $(1 - \epsilon_T)$ . For the lower temperature  
 383 bounds, the chance constraint can thus be written as:

$$Pr(\underline{T}_{room} \leq T_{room}^{t+1}) \geq 1 - \epsilon_T. \quad (24)$$

384 Then, we rewrite it as:

$$Pr(\chi_T^{t+1} \leq 0) \geq 1 - \epsilon_T, \quad (25)$$

385 where  $\chi_T^{t+1} = \underline{T}_{room} - T_{room}^{t+1}$ . Let the indoor temperature be rewritten in terms of the prediction  
 386 error:  $T_{room}^t = T_{room,f}^t + T_{room,e}^t$  where  $T_{room,f}^t$  is the predicted indoor room temperature and  
 387  $T_{room,e}^t$  is the error caused by uncertainties. Similarly,  $T_{room}^{t-1} = T_{room,f}^{t-1} + T_{room,e}^{t-1}$ . For both  
 388 timesteps, the room temperature distribution error follows the same distribution. The hypothetical  
 389 error distributions can be in different forms and here we assume the distribution to be normal.  
 390 Hence, it can be represented by:

$$T_{room,e}^{t,t-1} \sim \mathcal{N}(\mu_T^t, (\sigma_T^t)^2). \quad (26)$$

391 Therefore,  $\chi_T^{t+1}$  is also normally distributed with the following mean  $\mu^t$  and standard deviation  $\sigma^t$ :

$$\mu^t = \underline{T}_{room} - \beta_1(T_{room}^t + \mu_T^t) - \beta_2(T_{room}^{t-1} + \mu_T^t) - \beta_3 T_{amb}^t - \beta_4 T_{amb}^{t-1} - \beta_5 r_{hvac}^t - \beta_6 Q_{sol}^t - \beta_7 Q_{sol}^{t-1} - \beta_8 Q_{gain}^t - \beta_9 Q_{gain}^{t-1}, \quad (27)$$

$$\sigma^t = \sqrt{(\beta_1 \sigma_T^t)^2 + (\beta_2 \sigma_T^t)^2}. \quad (28)$$

392 The chance constraint can thus be reformulated as:

$$Pr(\chi_T^{t+1} \leq 0) = \Phi\left(\frac{0 - \mu^t}{\sigma^t}\right) \geq 1 - \epsilon_T, \quad (29)$$

393 where  $\Phi(\cdot)$  is the cumulative distribution function (CDF) of the standard normal distribution

394  $\mathcal{N}(0, 1)$ . By taking the inverse CDF of both sides, we can get:

$$\frac{0 - \mu^t}{\sigma^t} \geq \Phi^{-1}(1 - \epsilon_T). \quad (30)$$

395 Rearrange the above equation and substitute  $\mu^t$  and  $\sigma^t$  with Equations (27) and (28). Finally, we

396 obtain the chance constraint for ensuring the indoor temperature will not fall below the lower

397 bound of  $\underline{T}_{room}$  with the probability of  $(1 - \epsilon_T)$  as follows:

$$\begin{aligned} & \beta_1(T_{room}^t + \mu_T^t) + \beta_2(T_{room}^{t-1} + \mu_T^t) + \beta_3 T_{amb}^t + \beta_4 T_{amb}^{t-1} + \beta_5 r_{hvac}^t + \beta_6 Q_{sol}^t + \beta_7 Q_{sol}^{t-1} \\ & + \beta_8 Q_{gain}^t + \beta_9 Q_{gain}^{t-1} - \underline{T}_{room} \geq \Phi^{-1}(1 - \epsilon_T) \sqrt{(\beta_1 \sigma_T^t)^2 + (\beta_2 \sigma_T^t)^2}. \end{aligned} \quad (31)$$

398 Substituting Equation (3) into (31) and rearranging, we have:

$$T_{room}^{t+1} - \underline{T}_{room} \geq \Phi^{-1}(1 - \epsilon_T) \sqrt{(\beta_1 \sigma_T^t)^2 + (\beta_2 \sigma_T^t)^2} - (\beta_1 \mu_T^t + \beta_2 \mu_T^t). \quad (32)$$

399 Similarly, we have Equation (33) for the upper bound,

$$Pr(\bar{T}_{room} \geq T_{room}^{t+1}) \geq 1 - \epsilon_T. \quad (33)$$

400 Taking a similar derivation process as that in Equations (24) to (32), we can obtain the chance

401 constraint for the temperature upper bound:

$$\bar{T}_{room} - T_{room}^{t+1} \geq \Phi^{-1}(1 - \epsilon_T) \sqrt{(\beta_1 \sigma_T^t)^2 + (\beta_2 \sigma_T^t)^2 + (\beta_1 \mu_T^t + \beta_2 \mu_T^t)}. \quad (34)$$

402 The updated inequivalent constraints indicate that the temperature bounds for the optimization  
 403 should be narrower than the original temperature bounds to account for the setpoint behavioral  
 404 uncertainty, which is consistent with the expectations. Note that because the uncertainty-dealing  
 405 method is focused on the temperature constraints, one possible limitation is that the above method  
 406 might have limited effect on the controller design for buildings that have larger thermal masses,  
 407 because the building temperature is insensitive to temperature constraints. More discussion of this  
 408 point follows in Section 5.3.1.

## 409 5 Case Study

### 410 5.1 Studied Community

411 The case study community is a net-zero energy community located in Anna Maria Island, Florida,  
 412 USA, which is a cooling dominated region. The community buildings are installed with both roof-  
 413 top PV panels and solar carports, which harvest about 85 MWh annually for the whole community.  
 414 A centralized ground source heat pump system provides the HVAC needs of the whole community  
 415 with high efficiency. Other sustainable features include well-insulated building envelopes, solar  
 416 thermal water heating, and rainwater recycling. This community achieved net-zero energy in the  
 417 year of 2014. In the community, there are various building types such as residential, small office,  
 418 gift shop, etc. We would like to cover both residential and commercial buildings in the case study.  
 419 So, we selected one residential and two small commercial buildings based on the measurement  
 420 data quality. More specifically, the selected three buildings consist of a residential building (area:

421 93.8 m<sup>2</sup>), an ice cream shop (area: 160.5 m<sup>2</sup>), and a bakery (area: 410 m<sup>2</sup>). The building layout of  
 422 the community can be found in reference [28].  
 423 For the given community, a virtual testbed based on the object-oriented modeling language  
 424 Modelica [41] was built and validated [42]. In the testbed, the Typical Meteorological Year 3 data  
 425 for a nearby city, Tampa, was adopted for this case study. The building thermal models are  
 426 resistance-capacitance (RC) network models. For the optimal control in this work, the HVAC  
 427 models were trained using one month (i.e., August) of the simulation data exported from the  
 428 testbed. Table 2 lists the coefficients for the linear regression HVAC models, the Root Mean  
 429 Square Error (RMSE) of the models, as well as the corresponding nominal heat pump power. The  
 430 N/A in the table represents a coefficient that is too small and thus has been neglected in the model.  
 431 Three effective decimal places are provided.

432 *Table 2 Coefficients and nominal power of the HVAC models.*

		<b>Residential</b>	<b>Ice Cream Shop</b>	<b>Bakery</b>
<b>Coefficients</b>	$T_{room}^t$	1.429	0.502	0.977
	$T_{room}^{t-1}$	-0.432	0.498	0.0213
	$T_{amb}^t$	0.0263	0.000295	0.00405
	$T_{amb}^{t-1}$	-0.0232	-0.000193	-0.00196
	$r_{hvac}^t$	-0.210	-0.0114	-0.178
	$Q_{sol}^t$	0.0151	0.0000345	0.0107
	$Q_{sol}^{t-1}$	-0.00302	0.000181	-0.00621
	$Q_{gain}^t$	0.00852	N/A	N/A
	$Q_{gain}^{t-1}$	N/A	N/A	0.0140
<b>RMSE [°C]</b>		0.160	0.0205	0.114
<b>Nominal Power [kW]</b>		2.140	2.830	3.770

433

434 Additionally, Table 3 lists the load categorization for the studied buildings following the principles  
 435 proposed in Section 3.2. A complete list of the building load capacities and their heat gains can be  
 436 found in Appendix A.

437 *Table 3 Building loads categorized into four types.*

	<b>Residential</b>	<b>Ice Cream Shop</b>	<b>Bakery</b>
<b>Sheddable</b>	Computer	Coffee maker, soda dispenser, outdoor ice storage	Microwave
<b>Modulatable</b>	HVAC	HVAC	Mixer, unspecific room plug loads, HVAC
<b>Shiftable</b>	Range, washer, dryer	None	Range, oven, dishwasher
<b>Critical</b>	Lights, refrigerator	Lights, cooler, display case	Lights, cooler, display case

438  
 439 We designed three uncertainty levels (i.e., low, medium, high) as in Table 1 to evaluate the  
 440 deterministic and preference-aware schedulers in this paper. They are compared to the baseline  
 441 scenario, where the deterministic scheduler is applied without occupant behavior uncertainties.  
 442 The following results and discussion are all based on these scenarios. All scenarios were run in the  
 443 three buildings for 48 hours with a timestep of 1 hour in the islanded mode.

## 444 5.2 Settings of Chance-Constrained Controllers for Different Buildings

445 The preference-aware schedulers use chance-constrained controllers, whose settings depend on  
 446 individual building properties and uncertainty levels. Following the method proposed in Section  
 447 4.2.3, this section provides the details of the chance-constrained controller settings for three  
 448 individual buildings in the case study, which is based on the control outcome of the deterministic  
 449 schedulers under three uncertainty levels.

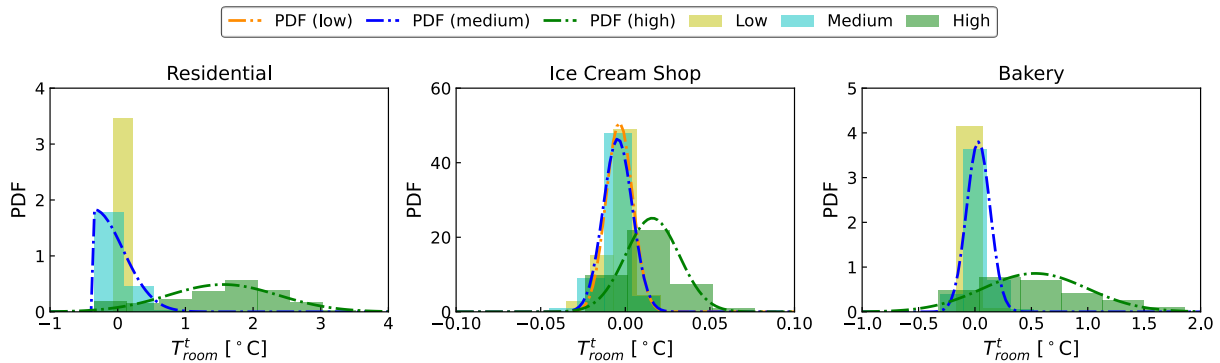
450 Considering the occupant-preference-driven actions as the source of “prediction errors” for the  
451 room temperature, we extracted the distributions of the room temperature prediction errors. The  
452 Monte Carlo simulation method [43] was adopted, where 100 repeated simulations were run using  
453 the deterministic scheduler with three uncertainty levels. We used the room temperature of the  
454 deterministic baseline scenario as the benchmark to calculate the errors caused by the occupant  
455 setpoint-changing behavior. To describe the room temperature errors, three hypothetical  
456 distributions are proposed (i.e., fit distribution in Table 4). The normal distribution is mentioned  
457 in the derivation in Section 4.2.3. The half-normal distribution is a fold of a normal distribution at  
458 its mean. For the residential building medium uncertainty level, a half-normal distribution was  
459 adopted. This can be attributed to the fact that almost no temperature decrease action was observed  
460 and thus the errors were all above zero. Constants were used for the residential building and the  
461 bakery under the low uncertainty level because the frequency of the setpoint-changing is too low  
462 (nearly zero) to follow any distributions.

463 Chi-square goodness of fit tests [44] at a rejection level of 1% were conducted to evaluate whether  
464 the proposed hypothetical distributions fit well. The types of fitting distributions, p-values of the  
465 tests, and the distribution parameters are reported in Table 4. In the table,  $\mu$  is the mean and  $\sigma$  is  
466 the standard deviation of the normal/half-normal distribution. The null hypothesis here is that the  
467 room temperature prediction error follows the hypothetical distribution. The p-value is the  
468 evidence against this null hypothesis. Since all p-values are greater than 99%, all error distributions  
469 failed to reject the hypothesis at the level of 1%. This means they all follow the corresponding  
470 hypothetical distribution.

471 *Table 4 Chi-square goodness of fit test p-values and normal distribution parameters.*

Building	Uncertainty	Fit Distribution	p-value	$\mu$ [°C]	$\sigma$ [°C]
Residential	Low	Constant	1.0	-6.45E-05	N/A
	Medium	Half-normal	0.999	-3.57E-01	4.35E-01
	High	Normal	0.999	1.56E+00	8.17E-01
Ice Cream Shop	Low	Normal	0.999	-3.48E-03	7.86E-03
	Medium	Normal	0.999	-4.45E-03	8.59E-03
	High	Normal	0.999	1.60E-02	1.59E-02
Bakery	Low	Constant	1.0	-3.42E-03	N/A
	Medium	Normal	0.999	3.01E-02	1.05E-01
	High	Normal	0.999	5.33E-01	4.65E-01

472 The frequency histogram and probability density functions (PDFs) of each building under various  
473 uncertainty levels are plotted in Figure 6. In the figure, it can be seen that the higher the uncertainty,  
474 the wider the room temperature range. This is because in scenarios with a higher uncertainty,  
475 occupants change the thermostat more frequently, which expands the possible temperature ranges.  
476 We also noticed that the temperature range in the ice cream shop is relatively concentrated  
477 compared to the other two buildings. This can be attributed to the large thermal mass of the  
478 building.



479  
480 *Figure 6 Room temperature prediction error PDFs obtained from the Monte Carlo simulations.*

481 For the scenario where the temperature prediction error follows the half-normal distribution, we  
482 applied the chance constraint only to the upper bound because only increasing actions happen in

483 this scenario. For the two scenarios where the room temperature error is estimated to be a constant,  
 484 we adopted the original temperature bounds of [20°C, 25°C] because the estimated errors in both  
 485 scenarios are smaller than 0.01°C. We choose the  $\epsilon_T = 1\%$  to ensure a 99% probability of  
 486 abidance of the temperature constraints (Equation (24)). Table 5 lists the updated room  
 487 temperature lower and upper bounds for each building under different scenarios.

488 *Table 5 Room temperature bounds for chance-constrained optimizations.*

<b>Building</b>	<b>Uncertainty</b>	<b><math>\underline{T}_{room}</math> [°C]</b>	<b><math>\overline{T}_{room}</math> [°C]</b>
<b>Residential</b>	Low	20.000	25.000
	Medium	20.000	24.236
	High	20.547	21.343
<b>Ice Cream Shop</b>	Low	20.024	24.983
	Medium	20.027	24.982
	High	20.025	24.943
<b>Bakery</b>	Low	20.000	25.000
	Medium	20.240	24.700
	High	20.664	23.273

489

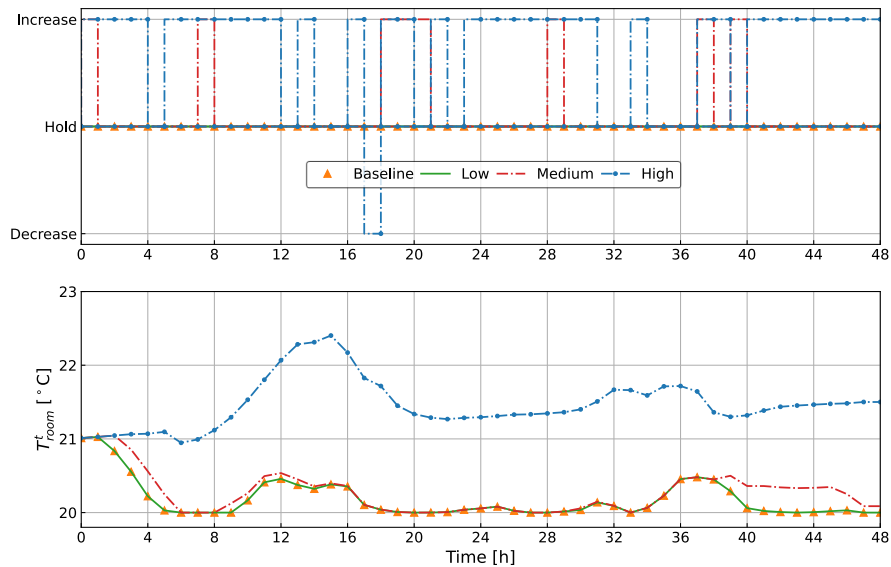
### 490 5.3 Results and Discussions

491 This section first quantifies the impact of introducing occupant behavior uncertainties to the  
 492 optimal scheduling problem. Then, the deterministic and chance-constrained controllers are tested  
 493 on the community virtual testbed. Their control performance in terms of the unserved load ratio,  
 494 the required battery size, and the unmet thermal preference hours are then compared.

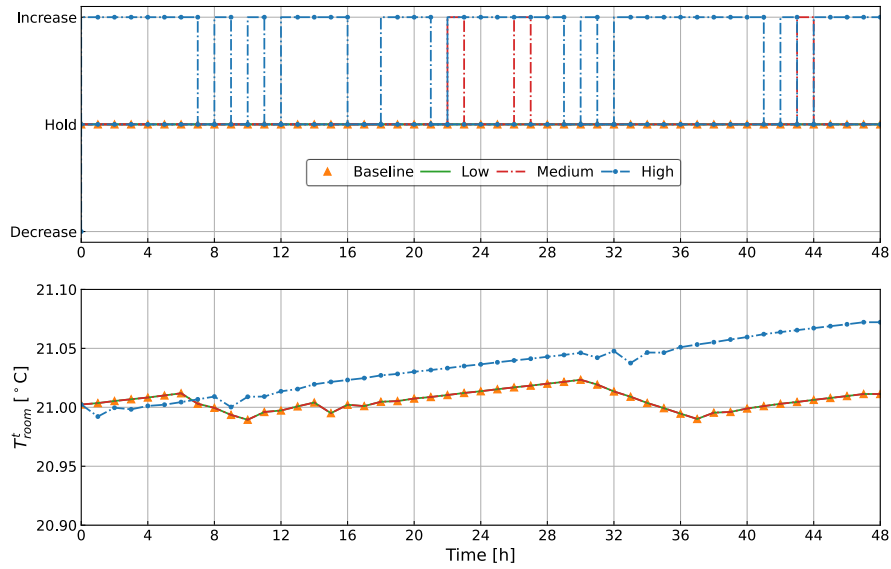
#### 495 5.3.1 Impact of Uncertainty

496 Figures 7 to 9 depict the occupant thermal preference and the corresponding room temperatures.  
 497 In the figures, the upper plots show the simulated stochastic thermostat-changing actions at

498 different uncertainty levels, where increase means a setpoint increase action, and vice versa. The  
 499 lower plots show the resulting room temperatures with dashed lines.  
 500 The results of the low uncertainty scenario overlap with that of the baseline scenario (i.e., the  
 501 deterministic scheduler without uncertainty) mainly due to the low probability of setpoint-  
 502 changing actions in this scenario. With the increase in the probability, we see more frequent  
 503 setpoint-changing actions in all three buildings. Further, the increase action happens more  
 504 frequently than the decrease action. This is because between the temperature range of 20°C and  
 505 24°C, the probability of increase is much higher than that of decrease (see Figure 4). This also  
 506 implies that the occupants' temperature preference is closer to 24°C than 20°C. Additionally, for  
 507 the residential building and the bakery, the temperature difference between scenarios is more  
 508 noticeable than for the ice cream shop; this is attributable to the different building thermal masses  
 509 of the three buildings.



510  
 511 *Figure 7 Residential building occupant thermostat changing actions (upper) and resulting room*  
 512 *temperatures (lower) under three levels of uncertainty.*



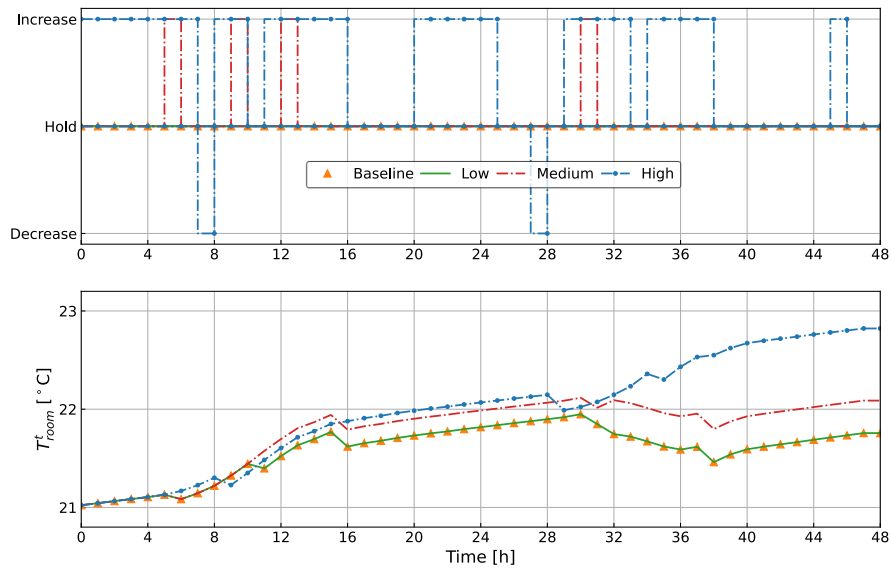
513

514

*Figure 8 Ice cream shop occupant thermostat changing actions (upper) and resulting room*

515

*temperatures (lower) under three levels of uncertainty.*



516

517

*Figure 9 Bakery occupant thermostat changing actions (upper) and resulting room temperatures*

518

*(lower) under three levels of uncertainty.*

519 Table 6 lists the values of the KRIs in correspondence with Figures 7 to 9. The HVAC energy and  
 520 average room temperature over the optimization horizon are also provided to facilitate the analysis  
 521 of the results.

522 *Table 6 Key resilience indicators for studied buildings under different uncertainty levels.*

Building	Scenario	Unserved Load Ratio	Battery Size [kWh]	HVAC Energy [kWh]	Mean Room Temperature [°C]
Residential	Baseline	0.0744	47.686	32.139	20.185
	Low	0.0744	47.686	32.139	20.185
	Medium	0.0744	47.168	32.099	20.271
	High	0.0744	38.541	21.400	21.468
Ice Cream Shop	Baseline	0.0215	99.139	32.703	21.006
	Low	0.0215	99.139	32.703	21.006
	Medium	0.0215	99.139	32.703	21.006
	High	0.0215	93.166	10.063	21.033
Bakery	Baseline	0.0247	80.007	35.144	21.579
	Low	0.0247	80.007	35.144	21.579
	Medium	0.0247	73.496	27.604	21.766
	High	0.0247	76.801	11.310	21.973

523  
 524 From the table, we see that the unserved load ratio remains the same across all scenarios for each  
 525 building. This can be attributed to the fact that in the controller design phase, the optimization  
 526 objective is set to minimize the unserved load ratio. Hence, the unserved load ratios for each  
 527 building are already minimal and are not affected by the occupants' thermostat-overriding  
 528 behavior uncertainties. Instead, the battery-charging/discharging behavior is affected, as reflected  
 529 by the different required battery sizes in the table. Note that the unserved load ratios are minimal,  
 530 but not zero, because of our assumption that each shiftable load operates once and only once per  
 531 day.

532 For the rest of the metrics, note that the battery size, HVAC energy, and the average room  
 533 temperature remain the same for the baseline and low uncertainty scenarios in all buildings. This

534 is because no setpoint-changing actions happened due to the relatively low probabilities, as shown  
535 in the figures above. As for the medium uncertainty scenarios, both the residential building and  
536 the bakery show higher room temperatures and lower HVAC energy while the ice cream shop still  
537 has the same results as the baseline, given its large thermal mass.

538 In terms of the high uncertainty scenarios, due to the prominent increase in room temperatures, we  
539 noticed more HVAC energy savings in all buildings. Note that though the average room  
540 temperature increase is insignificant, the HVAC energy savings is large due to the cumulative  
541 effect over the many hours of setpoint increase. Overall, we see a positive correlation between the  
542 HVAC energy and the required battery size. When the PV generation and the other building loads  
543 remain the same, the more HVAC energy, the larger required battery size. However, one opposite  
544 case was noted in the bakery high uncertainty scenario where the required battery size is slightly  
545 larger in the high uncertainty scenario than in the medium uncertainty scenario. This was caused  
546 by a setpoint decrease action at hour 28, which resulted in a battery discharging during the night  
547 and thus a smaller minimum SOC of the battery.

548 To summarize, occupant thermostat-changing behavior uncertainty needs to be considered when  
549 designing optimal schedulers for resilient buildings because it affects the indoor room temperature,  
550 the HVAC power, and thus the sizing of batteries. For the whole community, when considering  
551 the highest occupant behavior uncertainty, the consumed HVAC energy can be 57.2% less and the  
552 battery 8.08% smaller. Whereas the aforementioned impact depends on the uncertainty level (i.e.,  
553 how frequently the occupants change the setpoint), heating or cooling season, and the occupants'  
554 actual preference for the indoor room temperature compared to the room temperature designed by

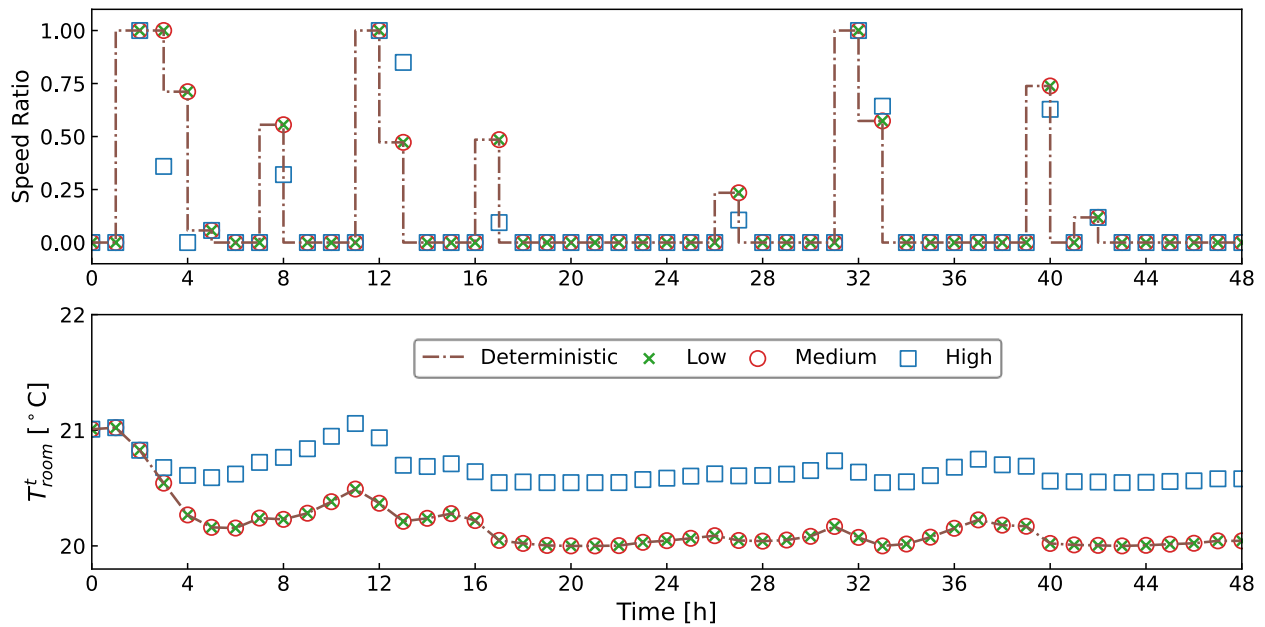
555 the scheduler. In our case, a preferred higher indoor room temperature saves HVAC energy.  
556 During the heating season, the observations could be the reversed.

### 557 5.3.2 Controller Performance

558 To further evaluate the performance of the chance-constrained controller in comparison with the  
559 deterministic controller, tests were run on the virtual testbed [28] in a stochastic manner. In each  
560 of the studied buildings, both the deterministic controller and the chance-constrained controller  
561 were tested for two days (i.e., August 4 and 5) with the three levels of uncertainties. The testing  
562 method is similar to the method proposed in Section 4.2.2. Additionally, the precalculated optimal  
563 battery charging/discharging, as well as the optimized loads, are also implemented in the testbed.  
564 One hundred repeated Monte Carlo simulations were run for each scenario to better observe the  
565 controller performance. The KRIs of the unserved load ratio, the required battery size, and the  
566 unmet thermal preference hours are adopted for the performance evaluation.

567 The upper plot of Figure 10 depicts the predetermined optimal schedules of the heat pump speed  
568 ratio as the inputs of the test. The lower plot then shows the corresponding room temperatures  
569 predicted by the linear regression models in the optimization. The data for the residential building  
570 is adopted here for the analysis. The plots for the ice cream shop and the bakery can be found in  
571 Appendix A. From the figure, we see that the scheduled speed ratios in the low and medium  
572 uncertainty scenarios overlap with that of the deterministic scheduler. Whereas the high  
573 uncertainty scenario tends to have lower speed ratios over the whole optimization horizon. This  
574 can be attributed to the controller settings shown in Table 5, where the temperature bounds set in  
575 the low and medium uncertainty scenarios are closer to the original bounds of [20°C–25°C]. Hence,  
576 the temperature constraints are not binding in these two scenarios. However, in the high

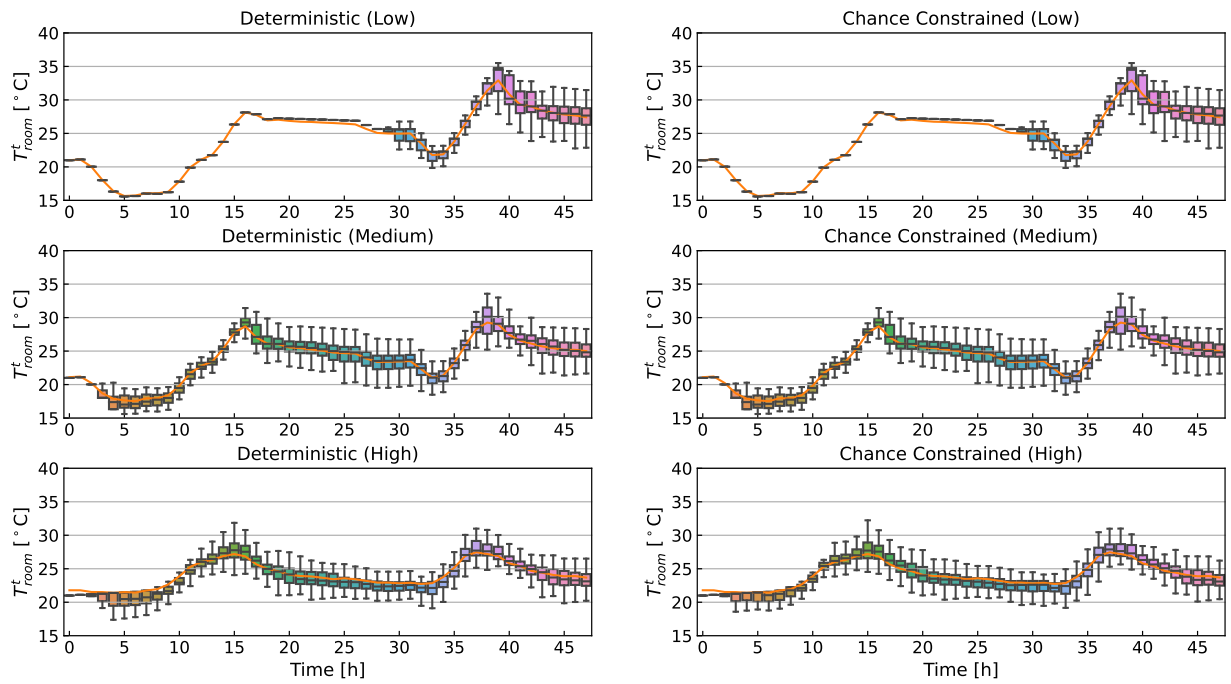
577 uncertainty scenario, the temperature constraint is binding, which leads to the speed ratio  
 578 reductions. As a result, a higher room temperature can be seen in the high uncertainty scenario.



579  
 580 *Figure 10 Optimal schedules of the heat pump speed ratio and predicted room temperatures by*  
 581 *various schedulers (residential building).*

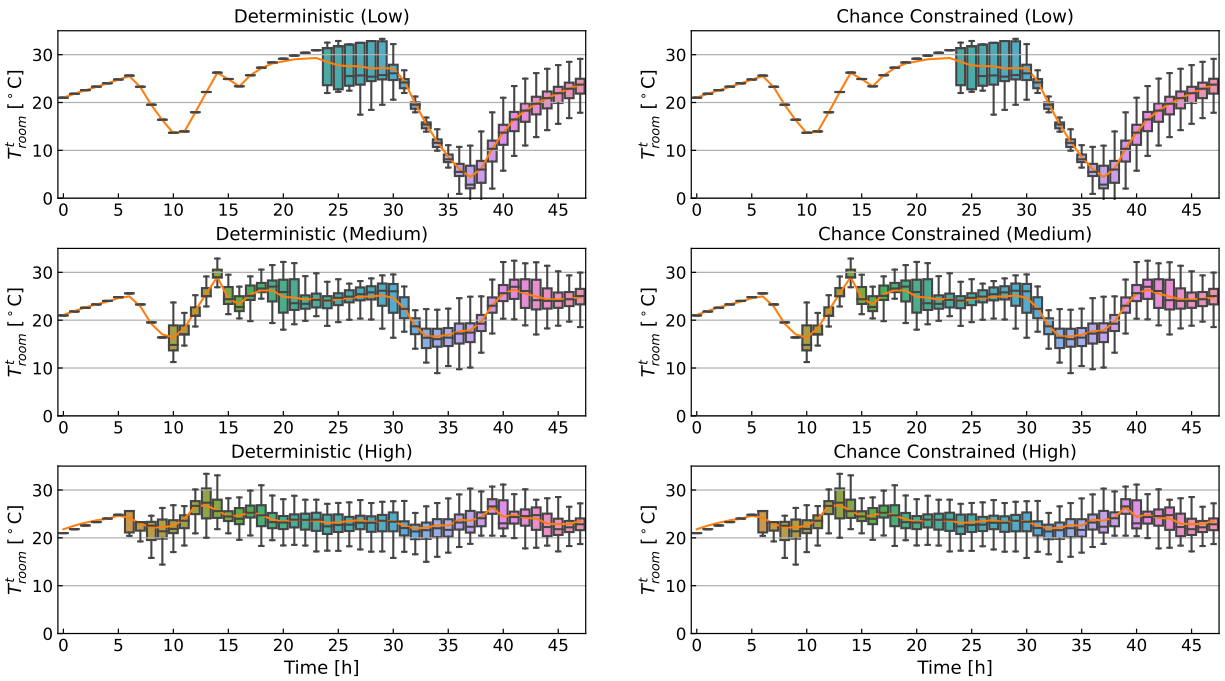
582 Figures 11 to 13 depict the room temperature boxplots as the controller testing outputs. The lower  
 583 and upper borders of the boxes represent the 25th and 75th percentiles of the data, respectively.  
 584 The longer the box, the more scattered the room temperature. The lines inside the boxes represent  
 585 the median values. The lines beyond the boxes represent the minimum and maximum values except  
 586 for outliers, which are not shown in these figures. Note in the figures that the temperatures first  
 587 concentrate together (shown as black lines) and then spread out (shown as boxes). This is because  
 588 at the beginning of the simulations, no overriding behavior of the setpoints happens and the heat  
 589 pump operates following the scheduled speed ratio. Once the overriding happens at a certain  
 590 timestep in some simulations, the room temperature trends start to deviate and become boxes. The

591 occupant-preferred temperature lines are also shown as orange lines in these figures as a reference;  
592 they are average setpoints adjusted by the occupants in all the Monte Carlo tests.



593

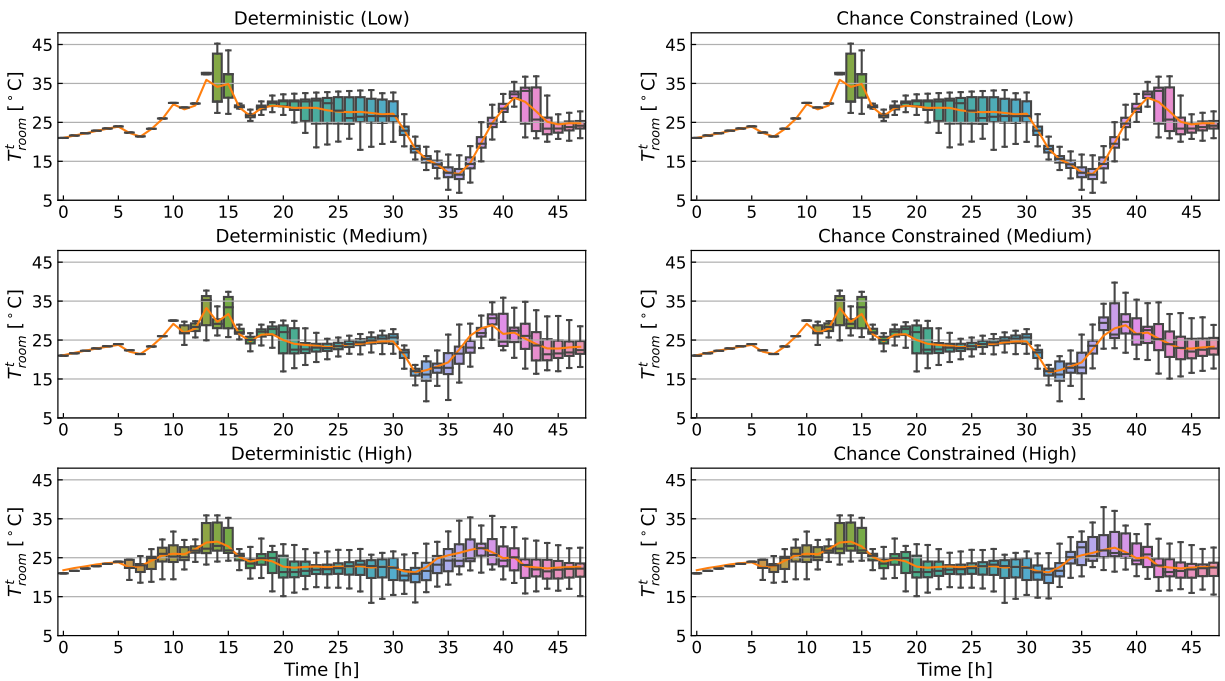
594 *Figure 11 Residential building room temperature boxplots for control testing results.*



595

596

Figure 12 Ice cream shop room temperature boxplots for control testing results.



597

598

Figure 13 Bakery room temperature boxplots for control testing results.

599 In the figures, we see a general trend of narrower room temperature ranges from the low  
600 uncertainty scenarios to high uncertainty scenarios. This is due to the introduction of the occupant  
601 setpoint-overriding mechanism, which tends to moderate the extreme room temperatures. Also,  
602 there is a plant-model mismatch, which describes the parametric uncertainty of modeling that  
603 originates from neglected dynamics of the plant [25]. In our case, the mismatch exists as the  
604 simulated room temperatures in the testbed are slightly higher than those predicted by the reduced-  
605 order linear HVAC models. This is understandable because the physics-based testbed has a much  
606 higher fidelity and simulates the non-linearity of the real mechanical systems.

607 Because the difference in the room temperature between the two controllers is not depicted in these  
608 figures, Table 7 and Table 8 provide further quantitative evaluations of the room temperatures  
609 along with other controller performance. Additionally, note that the optimal schedules of some  
610 scenarios remain the same because of the unbinding temperature constraints, which led to the same  
611 testing outputs. Here we only discuss the scenarios that have different inputs and outputs. A full  
612 list of all testing results is available in Table A-2.

613 *Table 7 Comparison of controller performance in the residential building high uncertainty*  
614 *scenario.*

<b>Controller</b>	<b>Unmet Thermal Preference Hours [°C·h]</b>	<b>Mean Room Temperature [°C]</b>	<b>Unserviced Load Ratio</b>	<b>Required Battery Size [kWh]</b>
Deterministic	48.91	23.75	0.074	47.69
Chance-constrained	46.42	23.87	0.074	44.12

615

616 In Table 7, we see a larger value of unmet thermal preference hours in the deterministic controller  
617 than the chance-constrained one. This can be attributed to the higher room temperatures regulated

618 by the chance constraints to better satisfy the occupants' thermal preferences. Again, the same  
 619 unserved load ratio is observed in both controllers because it is already minimal, which is enforced  
 620 by the objective function. In terms of the battery size, the chance-constrained controller shows a  
 621 smaller required battery size than the deterministic controller. This results from the fact that a  
 622 higher room temperature has led to less consumed HVAC energy in the chance-constrained  
 623 scenario. Thus, less discharging from the battery was happening, which led to a smaller required  
 624 battery size. For the bakery results shown in Table 8, the same trends for the battery size and the  
 625 unserved load ratio as the residential building can be observed under each uncertainty level.  
 626 Namely, smaller batteries and the same unserved load ratios.

627 *Table 8 Comparison of controller performances in the bakery medium and high uncertainty*  
 628 *scenarios.*

Uncertainty	Controller	Unmet Thermal Preference Hours [°C·h]	Mean Room Temperature [°C]	Unserved Load Ratio	Required Battery Size [kWh]
Medium	Deterministic	88.80	24.27	0.025	80.01
	Chance-constrained	91.28	24.50	0.025	76.89
High	Deterministic	102.81	23.65	0.025	80.01
	Chance-constrained	101.61	23.89	0.025	76.89

629  
 630 As for the unmet thermal preference hours, different trends are witnessed in the medium and high  
 631 uncertainty levels. In the medium level, the deterministic controller shows fewer unmet preference  
 632 hours than the chance-constrained controller. Whereas in the high uncertainty level, an opposite  
 633 trend is seen. This is reasonable as we see a generally higher mean room temperature regulated by  
 634 the chance-constrained controller under different uncertainty levels. However, in the medium  
 635 scenario, a lower preference temperature line was obtained from the Monte Carlo testing, which is

636 closer to the actual room temperatures of the deterministic controller. When the preference  
637 temperature rises in the high uncertainty scenario, the chance-constrained controller outperforms  
638 the deterministic controller with a higher actual room temperature and thus smaller unmet thermal  
639 preference hours.

640 When we compare different uncertainty levels in the bakery, we see that the mean room  
641 temperature decreases with the increase in uncertainty. This is because the lower temperature  
642 upper bounds shown in Table 5 have regulated the room temperature to sink when the uncertainty  
643 gets higher. Additionally, as seen in Figure 4, in the temperature range of 20°C to 24°C, the  
644 probability of increasing the temperature setpoint is much higher than that of decreasing it. While  
645 above 24°C, the probability to increase and to decrease is almost the same. This has caused the  
646 room temperatures to end up around 24°C in the high uncertainty scenarios for all buildings (Table  
647 A-2). This reveals that with the increase in the occupant thermostat-changing uncertainties, the  
648 room temperatures tend to get closer to the occupants' preferred room temperature.

649 Though some improvement was noticed in the chance-constrained controller compared to the  
650 deterministic controller, the overall improvement was less than expected. This could be attributed  
651 to the following three factors. First, the impact of the uncertainty level on the controller  
652 performance improvement is prominent as we observe higher performance improvement in high  
653 uncertainty scenarios. Second, the thermal property, especially thermal mass, of the building itself  
654 also affects the results. Thermal mass serves as a thermal buffer to filter the impact of various  
655 HVAC supply temperatures. Hence, buildings with a larger thermal mass tend to experience less  
656 impact from the occupant thermal preference uncertainty. This can be demonstrated by the results  
657 of the ice cream shop, where the two controllers perform the same. Third, the plant-model

658 mismatch also plays a significant role in the transition from the optimal scheduler design to its  
659 implementation. In the design phase, a series of control-oriented linear regression building models  
660 was used. However, the testing took place on a high-fidelity physics-based testbed, where the  
661 complex system dynamics of the whole buildings and HVAC systems were modeled with shorter  
662 simulation timesteps. This is a common source of uncertainty to be addressed for MPC design and  
663 implementation.

664 In our opinion, joint effort from building scientists, modelers, and engineers is needed to facilitate  
665 implementing stochasticity in the building domain and ultimately better serve the occupants. For  
666 example, an open-source database focused on building performance related stochasticity such as  
667 the occupant behavior and weather forecast needs to be established. Further, readily available  
668 stochastic simulation tools need to be developed (e.g., Occupancy Simulator [45]). Finally,  
669 stochasticity needs to be incorporated into the whole process of building modeling and design in  
670 the form of boundary conditions or internal components.

## 671 6 Conclusion

672 In this paper, we proposed a preference-aware scheduler for resilient communities. Stochastic  
673 occupant thermostat-changing behavior models were introduced into a deterministic load  
674 scheduling framework as a source of uncertainty. The impact of occupant behavior uncertainty on  
675 community optimal scheduling strategies was discussed. KRIs such as the unserved load ratio, the  
676 required battery size, and the unmet thermal preference hours were adopted to quantify the impacts  
677 of uncertainties. Generally, the proposed controller performs better in terms of the unmet thermal  
678 preference hours and the battery sizes compared to the deterministic controller. Though only tested  
679 on three buildings of the studied community, the methodology of introducing occupant behavior

680 uncertainty into load scheduling and testing can be generalized and applied to other building and  
681 behavior types.

682 More specifically, we determined that occupant thermostat-changing behavior uncertainty should  
683 be considered when designing optimal schedulers for resilient communities. For the whole  
684 community, when considering the highest occupant behavior uncertainty, the consumed HVAC  
685 energy can be 57.2% less and the battery 8.08% smaller. During the controller testing phase, the  
686 proposed chance-constrained controller proves its advantage over the deterministic controller by  
687 better serving the occupants' thermal needs and demonstrating a savings of 6.7 kWh of battery  
688 capacity for the whole community. Additionally, we noticed that with the presence of occupant  
689 thermostat-changing uncertainties, the room temperatures tend to get closer to the occupants'  
690 preferred room temperature.

691 During the simulation experiments, we noticed some limitations of the proposed work. Because  
692 the proposed uncertainty method mainly deals with the uncertainty through the temperature  
693 constraints, it can be less effective for buildings of larger thermal mass due to the insensitivity to  
694 temperature constraints. Also, plant-model mismatch was noticed in the controller testing phase,  
695 which is a common parametric uncertainty that originates from neglected dynamics of the  
696 plant [25]. Finally, we used the thermostat changing models developed based on data from private  
697 office spaces in different building types, which can be debatable. Future work for this research  
698 includes extending the scope to heating scenarios to further generalize the findings. Additionally,  
699 real-time MPC control techniques could be integrated into the framework to overcome the lack of  
700 flexibility in *a priori* designed controllers.

701 Acknowledgements

702 This research is partially supported by the National Science Foundation under Awards No. IIS-  
 703 1802017. It is also partially supported by the U.S. Department of Energy, Energy Efficiency and  
 704 Renewable Energy, Building Technologies Office, under Contract No. DE-AC05-76RL01830.  
 705 This work also emerged from the IBPSA Project 1, an internationally collaborative project  
 706 conducted under the umbrella of the International Building Performance Simulation Association  
 707 (IBPSA). Project 1 aims to develop and demonstrate a BIM/GIS and Modelica Framework for  
 708 building and community energy system design and operation.

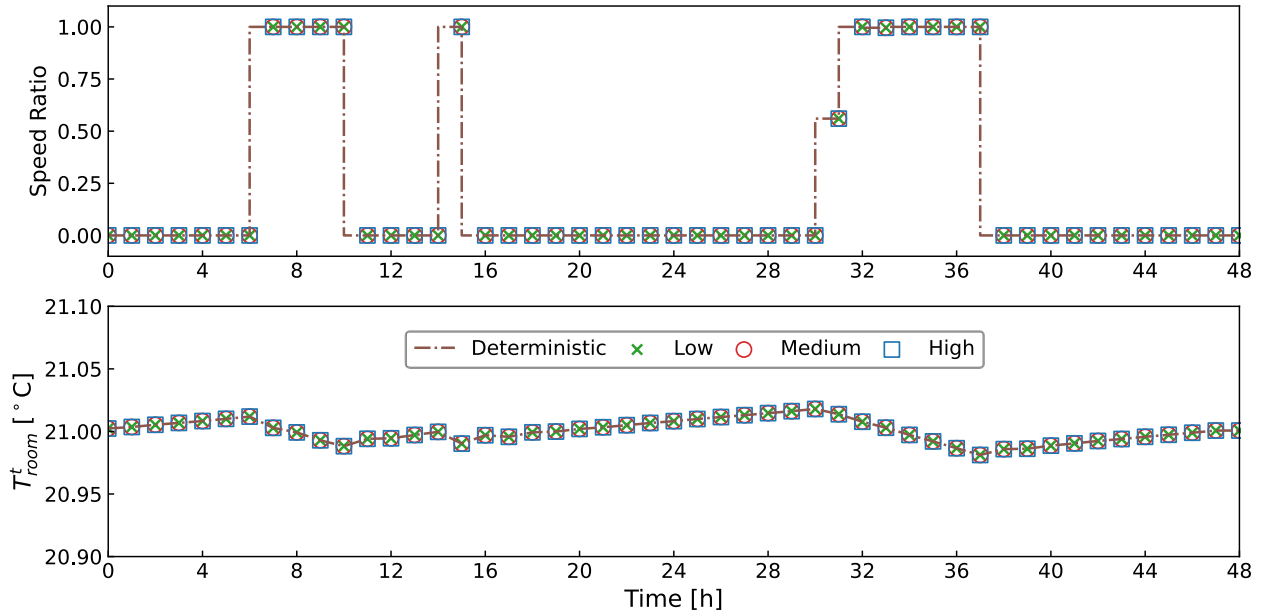
709 Appendix A

710 *Table A-1 Complete list of building loads and heat gain coefficients [31–33].*

Building	No.	Load	Capacity [W]	Heat Gain Coefficient	Heat Gain [W]	Weighted Average Coefficient
Residential	1	Lights	293	0.8	234.4	0.31
	2	Refrigerator	494	0.4	197.6	
	3	Computer	18	0.15	2.7	
	4	Range	1775	0.34	603.5	
	5	Washer	438	0.8	350.4	
	6	Dryer	2795	0.15	419.25	
Ice Cream Shop	1	Lights	135	0.8	108	0.35
	2	Coolers	7394	0.4	2957.6	
	3	Display case	280	0.4	112	
	4	Coffee maker	2721	0.3	816.3	
	5	Soda dispenser	201	0.5	100.5	
	6	Outdoor ice storage	1127	0	0	
Bakery	1	Lights	1859	0.8	1487.2	0.38
	2	Coolers	4161	0.4	1664.4	
	3	Display case	1011	0.4	404.4	
	4	Range	4065	0.15	609.75	

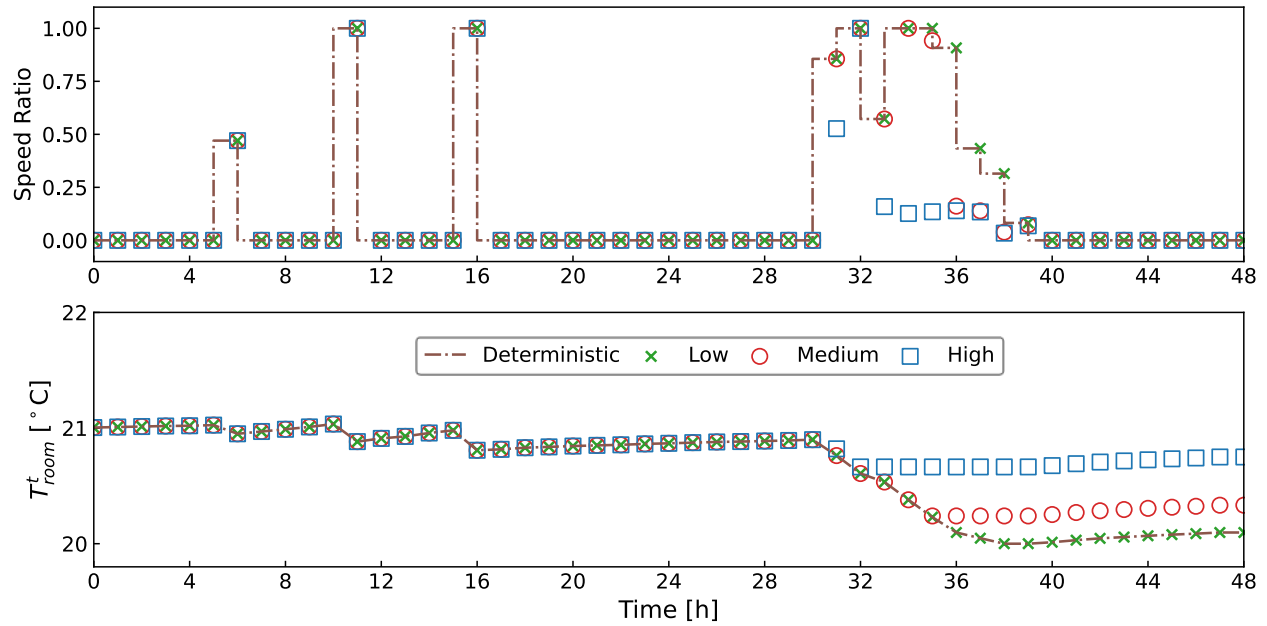
Building	No.	Load	Capacity [W]	Heat Gain Coefficient	Heat Gain [W]	Weighted Average Coefficient
	5	Mixer	521	0.31	161.51	
	6	Gas oven	761	0.2	152.2	
	7	Room plugs	377	0.5	188.5	
	8	Microwave	1664	0.67	1114.88	
	9	Dishwasher	1552	0.15	232.8	

711



712

713 *Figure A-1 Optimal schedules of the heat pump speed ratio and predicted room temperatures by*  
714 *various schedulers (ice cream shop).*



715

716 *Figure A-2 Optimal schedules of the heat pump speed ratio and predicted room temperatures by*  
 717 *various schedulers (bakery).*

718 *Table A-2 Full comparison of controller performances under different uncertainty levels in all*  
 719 *three buildings.*

KRIs	Controller	Residential			Ice Cream Shop			Bakery		
		Low	Medium	High	Low	Medium	High	Low	Medium	High
<b>Unmet Thermal Preference Hours [°C·h]</b>	Deterministic	33.70	47.19	48.91	70.69	85.61	86.87	89.03	88.80	102.81
	Chance-constrained	33.70	47.19	46.42	70.69	85.61	86.87	89.03	91.28	101.61
<b>Mean Room Temperature [°C]</b>	Deterministic	24.38	23.69	23.75	21.23	22.87	23.38	25.34	24.27	23.65
	Chance-constrained	24.38	23.69	23.87	21.23	22.87	23.38	25.34	24.50	23.89
<b>Unservd Load Ratio</b>	Deterministic	0.074			0.022			0.025		
	Chance-constrained	0.074	0.074	0.074	0.022	0.022	0.022	0.025	0.025	0.025
<b>Required Battery Size [kWh]</b>	Deterministic	47.69			99.14			80.01		
	Chance-constrained	47.69	47.69	44.12	99.14	99.14	99.14	80.01	76.89	76.89

720       References

- 721 [1]   The Texas Tribune. Winter Storm 2021. <https://www.texastribune.org/series/winter-storm->  
722       power-outage/ (accessed Apr 1, 2021).
- 723 [2]   Wang, J.; Garifi, K.; Baker, K.; Zuo, W.; Zhang, Y. Optimal Operation for Resilient  
724       Communities through a Hierarchical Load Scheduling Framework. In *Proceedings of 2020*  
725       *Building Performance Analysis Conference & SimBuild; Virtual Conference, 2020.*
- 726 [3]   Wang, J.; Zuo, W.; Rhode-Barbarigos, L.; Lu, X.; Wang, J.; Lin, Y. Literature Review on  
727       Modeling and Simulation of Energy Infrastructures from a Resilience Perspective. *Reliab.*  
728       *Eng. Syst. Saf.*, **2019**, *183*, 360–373. <https://doi.org/10.1016/j.res.2018.11.029>.
- 729 [4]   Tang, H.; Wang, S.; Li, H. Flexibility Categorization, Sources, Capabilities and  
730       Technologies for Energy-Flexible and Grid-Responsive Buildings: State-of-The-Art and  
731       Future Perspective. *Energy*, **2020**, 119598. <https://doi.org/10.1016/j.energy.2020.119598>.
- 732 [5]   Kou, X.; Li, F.; Dong, J.; Olama, M.; Starke, M.; Chen, Y.; Zandi, H. A Comprehensive  
733       Scheduling Framework Using SP-ADMM for Residential Demand Response with Weather  
734       and Consumer Uncertainties. *IEEE Trans. Power Syst.*, **2020**.  
735       <https://doi.org/10.1109/TPWRS.2020.3029272>.
- 736 [6]   Faraji, J.; Ketabi, A.; Hashemi-Dezaki, H.; Shafie-Khah, M.; Catalão, J. P. S. Optimal Day-  
737       Ahead Self-Scheduling and Operation of Prosumer Microgrids Using Hybrid Machine  
738       Learning-Based Weather and Load Forecasting. *IEEE Access*, **2020**, *8*, 157284–157305.  
739       <https://doi.org/10.1109/ACCESS.2020.3019562>.

- 740 [7] Wang, J.; Garifi, K.; Baker, K.; Zuo, W.; Zhang, Y.; Huang, S.; Vrabie, D. Optimal  
741 Renewable Resource Allocation and Load Scheduling of Resilient Communities. *Energies*.  
742 2020. <https://doi.org/10.3390/en13215683>.
- 743 [8] Yu, M. G.; Pavlak, G. S. Assessing the Performance of Uncertainty-Aware Transactive  
744 Controls for Building Thermal Energy Storage Systems. *Appl. Energy*, **2021**, 282, 116103.  
745 <https://doi.org/10.1016/j.apenergy.2020.116103>.
- 746 [9] Liang, Z.; Huang, C.; Su, W.; Duan, N.; Donde, V.; Wang, B.; Zhao, X. Safe Reinforcement  
747 Learning-Based Resilient Proactive Scheduling for a Commercial Building Considering  
748 Correlated Demand Response. *IEEE Open Access J. Power Energy*, **2021**, 8, 85–96.  
749 <https://doi.org/10.1109/oajpe.2021.3064319>.
- 750 [10] Ahmad, A.; Khan, J. Y. Real-Time Load Scheduling, Energy Storage Control and Comfort  
751 Management for Grid-Connected Solar Integrated Smart Buildings. *Appl. Energy*, **2020**,  
752 259, 114208. <https://doi.org/10.1016/j.apenergy.2019.114208>.
- 753 [11] E Silva, D. P.; Salles, J. L. F.; Fardin, J. F.; Pereira, M. M. R. Management of an Island and  
754 Grid-Connected Microgrid Using Hybrid Economic Model Predictive Control with  
755 Weather Data. *Appl. Energy*, **2020**, 278, 115581.  
756 <https://doi.org/10.1016/j.apenergy.2020.115581>.
- 757 [12] Yundra, E.; Surabaya, U. N.; Kartini, U.; Wardani, L.; Ardianto, D.; Surabaya, U. N.;  
758 Surabaya, U. N.; Surabaya, U. N. Hybrid Model Combined Fuzzy Multi-Objective Decision  
759 Making with Feed Forward Neural Network (F-MODMFFNN) For Very Short-Term Load

- 760 Forecasting Based on Weather Data. *Int. J. Intell. Eng. Syst.*, **2020**, *13* (4), 182–195.  
761 <https://doi.org/10.22266/IJIES2020.0831.16>.
- 762 [13] Garifi, K.; Baker, K.; Christensen, D.; Touri, B. Stochastic Home Energy Management  
763 Systems with Varying Controllable Resources. In *2019 IEEE Power & Energy Society  
764 General Meeting (PESGM)*; IEEE: Atlanta, GA, USA, 2019; pp 1–5.
- 765 [14] Lu, M.; Abedinia, O.; Bagheri, M.; Ghadimi, N.; Shafie-khah, M.; Catalão, J. P. S. Smart  
766 Load Scheduling Strategy Utilising Optimal Charging of Electric Vehicles in Power Grids  
767 Based on an Optimisation Algorithm. *IET Smart Grid*, **2020**, *3* (6), 914–923.  
768 <https://doi.org/10.1049/iet-stg.2019.0334>.
- 769 [15] Khalid, Z.; Abbas, G.; Awais, M.; Alquthami, T.; Rasheed, M. B. A Novel Load Scheduling  
770 Mechanism Using Artificial Neural Network Based Customer Profiles in Smart Grid.  
771 *Energies*, **2020**, *13* (5), 1062. <https://doi.org/10.3390/en13051062>.
- 772 [16] Kerboua, A.; Boukli-Hacene, F.; Mourad, K. A. Particle Swarm Optimization for Micro-  
773 Grid Power Management and Load Scheduling. *Int. J. Energy Econ. Policy*, **2020**, *10* (2),  
774 71. <https://doi.org/10.32479/ijeep.8568>.
- 775 [17] Kaur, R.; Schaye, C.; Thompson, K.; Yee, D. C.; Zilz, R.; Sreenivas, R. S.; Sowers, R. B.  
776 Machine Learning and Price-Based Load Scheduling for an Optimal IoT Control in the  
777 Smart and Frugal Home. *Energy AI*, **2021**, *3*, 100042.  
778 <https://doi.org/10.1016/j.egyai.2020.100042>.
- 779 [18] Chung, H.-M.; Maharjan, S.; Zhang, Y.; Eliassen, F. Distributed Deep Reinforcement

- 780 Learning for Intelligent Load Scheduling in Residential Smart Grids. *IEEE Trans. Ind.*  
781 *Informatics*, **2020**, *17* (4), 2752–2763. <https://doi.org/10.1109/TII.2020.3007167>.
- 782 [19] Aftab, M.; Chen, C.; Chau, C.-K.; Rahwan, T. Automatic HVAC Control with Real-Time  
783 Occupancy Recognition and Simulation-Guided Model Predictive Control in Low-Cost  
784 Embedded System. *Energy Build.*, **2017**, *154*, 141–156.  
785 <https://doi.org/10.1016/j.enbuild.2017.07.077>.
- 786 [20] Lim, B.; Van Den Briel, M.; Thiébaux, S.; Backhaus, S.; Bent, R. HVAC-Aware Occupancy  
787 Scheduling. In *Proceedings of the AAAI Conference on Artificial Intelligence*; 2015; Vol.  
788 29.
- 789 [21] Jin, Y.; Yan, D.; Zhang, X.; An, J.; Han, M. A Data-Driven Model Predictive Control for  
790 Lighting System Based on Historical Occupancy in an Office Building: Methodology  
791 Development. In *Building Simulation*; Springer, 2020; pp 1–17.  
792 <https://doi.org/10.1007/s12273-020-0638-x>.
- 793 [22] Wang, J.; Zuo, W.; Huang, S.; Vrabie, D. Data-Driven Prediction of Occupant Presence and  
794 Lighting Power: A Case Study for Small Commercial Buildings. In *American Modelica*  
795 *Conference*; 2020.
- 796 [23] Chen, X.; Wang, Q.; Srebric, J. Model Predictive Control for Indoor Thermal Comfort and  
797 Energy Optimization Using Occupant Feedback. *Energy Build.*, **2015**, *102*, 357–369.  
798 <https://doi.org/10.1016/j.enbuild.2015.06.002>.
- 799 [24] West, S. R.; Ward, J. K.; Wall, J. Trial Results from a Model Predictive Control and

- 800 Optimisation System for Commercial Building HVAC. *Energy Build.*, **2014**, 72, 271–279.  
801 <https://doi.org/10.1016/j.enbuild.2013.12.037>.
- 802 [25] Drgoňa, J.; Arroyo, J.; Figueroa, I. C.; Blum, D.; Arendt, K.; Kim, D.; Ollé, E. P.; Oravec,  
803 J.; Wetter, M.; Vrabie, D. L. All You Need to Know about Model Predictive Control for  
804 Buildings. *Annu. Rev. Control*, **2020**. <https://doi.org/10.1016/j.arcontrol.2020.09.001>.
- 805 [26] Garifi, K.; Baker, K.; Touri, B.; Christensen, D. Stochastic Model Predictive Control for  
806 Demand Response in a Home Energy Management System. In *2018 IEEE Power & Energy  
807 Society General Meeting (PESGM)*; Portland, OR, USA, 2018; pp 1–5.
- 808 [27] Zhang, X.; Schildbach, G.; Sturzenegger, D.; Morari, M. Scenario-Based MPC for Energy-  
809 Efficient Building Climate Control under Weather and Occupancy Uncertainty. In *2013  
810 European Control Conference (ECC)*; IEEE, 2013; pp 1029–1034.
- 811 [28] He, D.; Huang, S.; Zuo, W.; Kaiser, R. Towards to the Development of Virtual Testbed for  
812 Net Zero Energy Communities. In *SimBuild 2016: Building Performance Modeling  
813 Conference*; Salt Lake City, UT, USA, 2016; Vol. 6.
- 814 [29] Zakula, T.; Armstrong, P. R.; Norford, L. Modeling Environment for Model Predictive  
815 Control of Buildings. *Energy Build.*, **2014**, 85, 549–559.  
816 <https://doi.org/10.1016/j.enbuild.2014.09.039>.
- 817 [30] The Engineering ToolBox. Metabolic Heat Gain from Persons.  
818 [https://www.engineeringtoolbox.com/metabolic-heat-persons-d\\_706.html](https://www.engineeringtoolbox.com/metabolic-heat-persons-d_706.html) (accessed Feb  
819 19, 2021).

- 820 [31] Hosni, M. H.; Beck, B. T. Updated Experimental Results for Heat Gain from Office  
821 Equipment in Buildings. *ASHRAE Trans.*, **2011**, *117* (2).
- 822 [32] ASHRAE. *ASHRAE Handbook — Fundamentals 2017*; 2017.
- 823 [33] Lawrence Berkeley National Laboratory. Home Energy Saver & Score: Engineering  
824 Documentation - Internal Gains. [http://hes-documentation.lbl.gov/calculation-](http://hes-documentation.lbl.gov/calculation-methodology/calculation-of-energy-consumption/heating-and-cooling-calculation/internal-gains)  
825 [methodology/calculation-of-energy-consumption/heating-and-cooling-](http://hes-documentation.lbl.gov/calculation-methodology/calculation-of-energy-consumption/heating-and-cooling-calculation/internal-gains)  
826 [calculation/internal-gains](http://hes-documentation.lbl.gov/calculation-methodology/calculation-of-energy-consumption/heating-and-cooling-calculation/internal-gains) (accessed Feb 16, 2021).
- 827 [34] Maslow, A. H. *Motivation and Personality*; Harper & Brothers: New York City, USA, 1954.
- 828 [35] Roth, A.; Reyna, J.; Christensen, J.; Vrabie, D.; Adetola, V. GEB Technical Report Webinar  
829 Series: Whole-Building Control, Sensing, Modeling & Analytics  
830 [https://www.energy.gov/sites/default/files/2020/05/f74/bto-geb-webinar-CSMA-](https://www.energy.gov/sites/default/files/2020/05/f74/bto-geb-webinar-CSMA-051920.pdf)  
831 [051920.pdf](https://www.energy.gov/sites/default/files/2020/05/f74/bto-geb-webinar-CSMA-051920.pdf).
- 832 [36] Zhao, Z.; Lee, W. C.; Shin, Y.; Song, K.-B. An Optimal Power Scheduling Method for  
833 Demand Response in Home Energy Management System. *IEEE Trans. Smart Grid*, **2013**,  
834 *4* (3), 1391–1400. <https://doi.org/10.1109/TSG.2013.2251018>.
- 835 [37] SiteSage. Historic Green Village Submetering Data.  
836 <https://sitesage.net/home/management/index.php> (accessed Oct 7, 2020).
- 837 [38] Garifi, K.; Baker, K.; Christensen, D.; Touri, B. Control of home energy management  
838 systems with energy storage: Nonsimultaneous charging and discharging guarantees

- 839 <https://arxiv.org/pdf/1805.00100.pdf>.
- 840 [39] Gunay, H. B.; O'Brien, W.; Beausoleil-Morrison, I.; Bursill, J. Development and  
841 Implementation of a Thermostat Learning Algorithm. *Sci. Technol. Built Environ.*, **2018**,  
842 *24* (1), 43–56. <https://doi.org/10.1080/23744731.2017.1328956>.
- 843 [40] Heirung, T. A. N.; Paulson, J. A.; O'Leary, J.; Mesbah, A. Stochastic Model Predictive  
844 Control—How Does It Work? *Comput. Chem. Eng.*, **2018**, *114*, 158–170.  
845 <https://doi.org/10.1016/j.compchemeng.2017.10.026>.
- 846 [41] The Modelica Association. Modelica. 2019.
- 847 [42] Huang, S.; Wang, J.; Fu, Y.; Zuo, W.; Hinkelman, K.; Kaiser, M. R.; He, D.; Vrabie, D. *An*  
848 *Open-Source Virtual Testbed for a Real Net-Zero Energy Community*; 2021.
- 849 [43] Mooney, C. Z. *Monte Carlo Simulation*; Sage, 1997.
- 850 [44] Statistics Solutions. Chi-Square Goodness of Fit Test.  
851 <https://www.statisticssolutions.com/chi-square-goodness-of-fit-test/> (accessed Feb 25,  
852 2021).
- 853 [45] Chen, Y.; Hong, T.; Luo, X. An Agent-Based Stochastic Occupancy Simulator. In *Building*  
854 *Simulation*; Springer, 2018; Vol. 11, pp 37–49.
- 855